U. PORTO
FEUP FACULDADE DE ENGENHARIA
UNIVERSIDADE DO PORTO

Master's in Mechanical Engineering

Machinability of Inconel 718 in milling operations using SiAlON tools

Filipa Moreira (up200304179@fe.up.pt)

Supervisor:
Tiago Silva

Co-supervisors:
Abílio Jesus
Vítor Sousa

September, 2024

Abstract

The machinability of Inconel 718, a high-performance superalloy widely used in aerospace and industrial applications, presents significant challenges due to its high hardness and low thermal conductivity. Milling is a crucial machining process for Inconel 718, yet it often leads to rapid tool wear and high cutting temperatures. To address these challenges, the use of advanced ceramic tools, particularly SiAlON, has been explored due to their exceptional hardness and thermal stability. This master's thesis investigates the machinability of Inconel 718 using SiAlON solid milling tools, aiming to identify effective strategies for improving tool performance and surface quality.

The influence of tool geometry has been investigated, using two distinct milling tools with 4 and 6 teeth. These tools were evaluated in both up-milling and down-milling operations, employing linear strategies. Additionally, a spiral facing down-milling strategy was investigated, as it demonstrated notable benefits in tool performance. The study also examined different parameter combinations, either maximizing radial or axial depth of cut, in order to determine their impact on machining efficiency and tool wear.

The findings reveal that down-milling with a spiral strategy offers significant advantages in terms of tool life and surface finish. Tools with 6 cutting edges showed lower average temperatures and reduced wear compared to those with 4 edges. Moreover, varying the cutting parameters revealed that combinations with lower axial depth of cut and higher radial depth of cut generally resulted in more controlled temperature profiles and improved machining outcomes.

This research contributes to a deeper understanding of Inconel 718 machining with SiAlON tools and provides practical insights into optimizing milling strategies to enhance tool performance and extend tool life.

Key words: Milling; Machinability; Inconel 718; SiAlON; Cutting forces; Surface integrity; Cutting temperature analysis; Cutting tool wear

Resumo

A maquinabilidade do Inconel 718, uma superliga de alto desempenho muito utilizada em aplicações aeroespaciais e industriais, apresenta grandes desafios devido à sua elevada dureza e baixa condutividade térmica. A fresagem de Inconel 718 é um processo de maquinagem essencial, ainda assim leva a um rápido desgaste das ferramentas de corte e a elevadas temperaturas de corte. De modo a responder a estes desafios, a utilização de ferramentas de corte cerâmicas, em particular SiAlON, tem sido explorada graças à sua excecional dureza e estabilidade térmica. Esta dissertação investiga a maquinabilidade do Inconel 718 utilizando fresas integrais de SiAlON, com o objetivo de identificar as estratégias capazes de melhorar o desempenho das ferramentas e a qualidade superficial das peças maquinadas.

Foi investigado o efeito da geometria da ferramenta de corte, tendo sido usadas fresas integrais com 4 e 6 gumes. Estas ferramentas foram empregues em operações de fresagem concordante e discordante com estratégia linear. Adicionalmente, foram analisadas operações de fresagem com estratégia de fresagem concordante em espiral, uma vez que se apresentou mais benefícios para o desempenho das ferramentas. Ainda foram estudadas diferentes combinações de parâmetros de corte, maximizando a profundidade axial ou radial, de forma a compreender o seu impacto na eficiência e desgaste das ferramentas.

Os resultados revelam que efetuar as operações de fresagem concordante com estratégia em espiral oferece vantagens significativas em termos de vida da ferramenta e acabamento da superfície. Fresas integrais com 6 arestas de corte apresentaram temperaturas médias menores e menor desgaste comparado com as ferramentas de 4 arestas de corte. Adicionalmente, percebeu-se que a combinação de baixas profundidades de corte axiais com um elevadas profundidades de corte radiais, em geral, resulta em temperaturas mais controladas e melhora o processo de maquinagem.

Este estudo contribui para um entendimento mais profundo sobre a maquinabilidade do Inconel 718 com ferramentas de SiAlON e providencia conhecimento prático sobre estratégias de otimização de operações de fresagem tendo em vista um melhor desempenho e uma vida da ferramenta maior.

Palavras-chave: Fresagem;Maquinabilidade; Inconel 718; SiAlON; Esforços de corte; Integridade superficial; Temperatura de corte; Desgaste de ferramentas

Para a Tatá

“ad augusta per angusta”

Acknowledgements

Ao Professor Abílio por, assim que o contactei, se ter mostrado disponível e entusiasmado com a minha possível participação nesta jornada. Sem ele nada teria começado.

Ao Tiago por toda a ajuda e empenho em me dar todas as ferramentas que precisei e por ter tornado todo o processo em algo leve e mágico. Sem ele nada se teria desenvolvido.

Ao Vítor por ter estado sempre lá, por ter sido a ponte entre os ídolos e o mundo terreno e por não ter permitido nunca que fosse um percurso solitário. Sem ele nada teria sido finalizado.

Aos três por terem sido quem verdadeiramente semeou todas as canções no vento que passou ao longo do meu percurso em Engenharia Mecânica.

Institutional Acknowledgements

The author gratefully acknowledges the funding of Project Hi-rEV – Recuperação do Setor de Componentes Automóveis (C644864375-00000002) cofinanced by Plano de Recuperação e Resiliência (PRR), República Portuguesa through NextGeneration EU.

Contents

List of Figures

List of Tables

Abbreviations, Acronyms and Letters

a_e - radial depth of cut
a_p - axial depth of cut
BUE - built-up edge
CVD - chemical vapor deposition
D - diameter
EDS - energy-dispersive X-ray spectroscopy
F_a - active cutting force
F_c - cutting force
F_{cn} - normal cutting force
FEM - finite element method
f_z - feed per tooth
F_z- axial force
HSS - high-speed steel
n - rotational speed of the tool
PCBN - polycrystalline cubic boron nitride
PVD - physical vapor deposition
RCD - rotating cutting force dynamometer
SEM - scanning electron microscope
v_c - cutting speed
v_f - feed rate
z - number of teeth

1 Introduction

1.1 Motivation

Nickel-based superalloys, first developed in the 1940s [1] present several challenges in its machining, essentially due to the combination of two factors: low thermal conductivity and high tendency to work harden. Inconel 718 is a nickel-chromium-iron alloy renowned for its high mechanical strength and exceptional thermal resistance, largely attributed to the presence of precipitates within the alloy's microstructure [2, 3]. In fact, this alloy retains high mechanical strength at high temperatures, corrosion resistance, a smooth ductile-fragile transition temperature and good creep resistance [4]. These properties make it an excellent choice for high demanding applications, such as aerospace engineering. In addition to its extensive use in this industry, Inconel 718 is also employed in other sectors such as energy and automotive industries, owing to its outstanding mechanical properties.

Machining, whether turning, milling or other operations, is crucial for these industries, as it makes it possible to obtain high dimensional, form and surface finish accuracy [5], while offering the possibility of addressing the urgent needs of systems that require maintenance or the replacement of precision components. Materials with low machinability, as is the case of Inconel 718, lead to less efficient processes in energy terms and, consequently, in economic terms. Not only because tool life tends to be shorter, but also because working time is increased, since traditional tooling options (i.e., carbide tools) are limited by very low speeds, particularly for thermal resistant materials, such as the Ni-based alloys. Additionally, both tungsten and cobalt, used in the manufacturing of carbide tools, are finite resources, and their extraction faces geopolitical and environmental challenges, leading to supply chain uncertainties and rising costs and increase the pressure on the industry to find sustainable and more affordable alternatives without compromising performance.

Studies into the use of cutting tools made of α/β-SiAlON in the machining, especially milling, of Inconel 718 have therefore been multiplying, largely due to the underlying promise of employing higher cutting speeds. Even though conventional CNC machines usually are limited to operate in 18000 rpm, this results in approximate cutting speeds of 500m/min for solid milling tools with diameters smaller than 10 mm, which can be used in pre-finishing and semi-roughing of complex parts. Those speeds are a 5 times increment to conventional cemented carbide tooling solutions. The use of high speeds is only possible because ceramics can maintain their mechanical properties even at high temperatures, as well as to resist abrasive wear and to be chemically stable. In that sense, the development of these ceramic cutting tools has been the subject of research, thanks to the economic and ecological potential that these tools can offer. In one hand, by achieving higher cutting speeds, the entire milling process becomes more productive, bringing economic gains. On the other hand, the possibility of milling in the total absence of cutting fluids, as well as the lower energy consumption in these operations, allow for environmental gains at the same time [6].

One issue that arises when machining material like Inconel 718 with carbide cutting tools is the need to use a large volume of cutting fluids, which act not only as a lubricant, that reduces friction between tool and workpiece, but also as a cooling agent, since the high generated cutting temperatures can compromise the performance of tools. Ceramic tools offer the possibility not only of operating without the use of cutting fluids, in dry milling, but also the advantage of, by not using any coolant, allowing temperatures to rise in the cutting processes and thus promoting the thermal softening of Inconel 718.

In this context, there is a need to explore academic studies on the use of tools made entirely of SiAlON in the milling of Inconel 718, to better understand the cutting forces and temperatures involved in these operations, the existing wear mechanisms and to find a combination of factors that allow the processes to be optimized.

1.2 Document structure

This document begins with chapter 1, giving an overview of the topics covered in the study, explaining the motivation behind the study and how it will be organized.

Chapter 2 discusses the challenges of machining Inconel 718, and the main aspects related to milling processes. It then addresses some characteristics of the tools used in milling, the use of SiAlON as an alternative to carbides in the manufacturing of these tools, and the main types and mechanisms of wear encountered during milling operations of Inconel 718.

Chapter 3 aims to present an overview of the studies found on the subject. It presents a short summary of the different studies carried out in the field of milling super alloys, particularly Inconel 718, with ceramic materials.

Chapter 4 presents the materials and methods used in this study, such as properties of Inconel 718 sample used, percentages of α/β-phases in solid milling tools and their geometry. Additionally, this chapter explains how the experimental setup was prepared for conducting the practical tests and how the data was acquired for subsequent analysis, concluding with the definition of the numerical model used in the simulation of the cutting process using FEM (Finite Element Method).

Chapter 5 presents the results obtained and its discussion. It begins with an analysis of the cutting forces, then tool wear is discussed, exploring the various wear mechanisms encountered, followed by an analysis of the surface integrity of the created surface, and finally, an analysis of the temperatures involved and a prediction of temperature and tool-workpiece interface pressure.

Finally, chapter 6 presents the conclusions reached after analyzing and discussing the results, as well as indicating relevant future studies to follow up on what has been developed.

2 Theoretical Introduction

2.1 Machining challenges of Inconel 718

In addition to nickel, chromium and iron, Inconel 718 has other dispersed alloying elements, which distinguish it from other nickel alloys, and some carbides, which give the alloy its highly abrasive behavior [3]. On the other hand, Inconel 718 high temperature resistance, which allows it to maintain its excellent mechanical properties, is attributed to the precipitation of a solid solution that prevents slipping of the crystal structure [7], acting as barrier to material deformation.

Both abrasive behavior and resistance to high temperatures influence the material's machinability, posing two major challenges. The first has to do with the difficulty of finding a tool material that yields an acceptable service life [2], since Inconel 718 tends to harden when machined [4], which can be minimized by cutting at higher speeds [4], as those allow the phenomenon of thermal softening to occur.

Above 750°C Inconel 718 shows some softening and its machinability increases [3]. However, under these conditions, an oxide layer is created on the surface of the workpiece [7], and the adhesion of the workpiece material to the tool is favored, also leading to excessive tool wear. Additionally, metallurgical damage to the machined part occurs, by means of distortion and residual stresses [2], caused by the high cutting forces generated in these processes [4], as well as distortions and the appearance of residual stresses [2]. The reasons why Inconel 718 is a material that poses many machining challenges can be summarized in the following list [1]:

- Strong tendency to form BUE (Built-Up Edge), since the material tends to stick to the tool during machining
- Hardening when being worked, which is one of the causes that leads to high cutting forces
- Rapid tool wear due to its abrasive particles
- High mechanical strength at high temperatures
- Low thermal conductivity, which leads to high temperatures in the cutting zone

2.2 Aspects of the milling process

Milling operations are a common industrial practice with regards to precision manufacturing [3]. In these operations, a rotating cutting tool, also known as milling cutter, with several main cutting edges, moves across the workpiece, with well-defined geometrical parameters, removing material as it advances [8]. Although the milling cut is oblique, it can be simplified and approximated to an orthogonal cut. The simplification of milling process is shown in Figure 2.1.

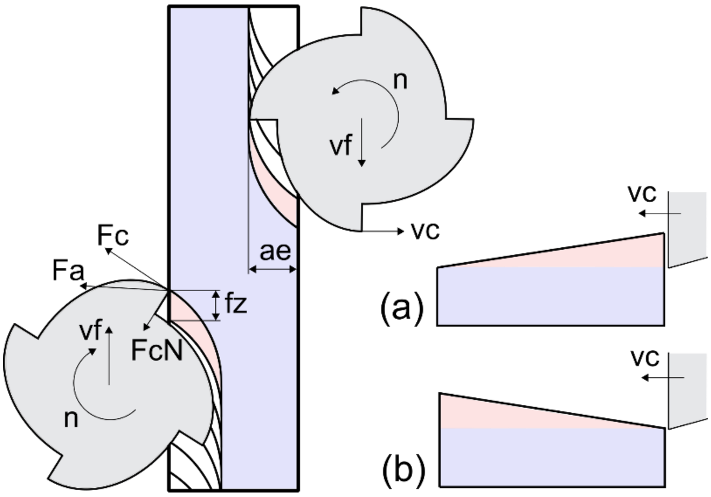

Figure 2.1: Scheme of the milling process and orthogonal cutting simplification of the down-milling (a) and up-milling (b) cutting strategies.

The cutting tool engages the workpiece with two specific depth parameters: the radial depth of cut (a_e) and the axial depth of cut (a_p). In this machining process, the cutting edge (and cutting tool) is intermittently exposed to high mechanical and thermal stress, which leads to less thermal damage compared to turning, but in turn results in greater deterioration of the cutting tools [3].

Tool loading scheme can be represented in an axis system defined according to the workpiece, where the forces involved can be divided in F_c, F_{cn} and F_z. F_c is the tangential force and acts tangentially to the cutter's rotation. It's the primary cutting force and is responsible for driving material removal and generating torque on the spindle. F_{cn} is the radial force that acts perpendicular to the axis of the tool and is responsible for the side deflection of the tool. Figure 2.1 shows how the cutting forces F_c and F_{cn}, related through the active cutting force, F_a. Thus, Equation 1, Equation 2 and Equation 3 show how these forces are related, and how they related to M_z.

$$F_a = \sqrt{{F_c}^2 + {F_{cn}}^2}$$ *Equation 1*

$$F_a = \sqrt{{F_c}^2 + {F_{cn}}^2}$$ *Equation 2*

$$F_c = \frac{M_z}{r}$$ *Equation 3*

Figure 2.1 also shows a representation of two key parameters for the machining process: cutting speed, v_c, and feed rate, v_f. In milling, v_c refers to the speed at which the cutting edge of the tool moves relative to the surface of the workpiece.

The cutting speed, v_c, is typically expressed in meters per minute (m/min). It is a critical parameter in machining because it directly influences the rate of material removal, tool wear, and surface finish. The cutting speed is determined by the rotational speed of the tool, n, (measured in revolutions per minute, or RPM) and the diameter of the cutting tool, D. Equation 4 enables its calculation.

The speed at which the workpiece is fed into the cutting tool, v_f, is typically measured in millimeters per minute (mm/min). It directly influences the machining time, the surface finish of the workpiece, the cutting forces, and the overall tool life. Equation 5 allows calculation of v_f, where f_z is feed per tooth, i.e., the distance the tool advances per revolution for each tooth, representing the amount of material (maximum chip thickness) that each tooth removes with every pass essentially, and z is the number of teeth.

$$v_c = \frac{D * \pi * n}{1000} \qquad \textit{Equation 4}$$

$$v_f = f_z * z * n \qquad \textit{Equation 5}$$

There are two types of milling operations which differ on the tool rotation direction relative to the feed direction of the workpiece: (i) down-milling and (ii) up-milling [9]. Figure 2.1 shows a simplification of the differences between the two. Down-milling (illustrated in Figure 2.1a) is characterized by the direction of rotation of the tool being the same as that of the feed, with the chip having its maximum size at the start of the cut on each tooth and gradually decreasing until it is theoretical zero. Up-milling, on the other hand, has the opposite direction of rotation of the cutter and the feed, with the chip starting at minimum thickness and gradually increasing until the end of each tooth's passage [10], as seen in Figure 2.1b.

2.3 Milling cutting tools

The ideal cutting tool should have high hardness, toughness, mechanical strength, be chemically inert, withstand cyclical mechanical and thermal loads and have the ability to retain cutting edge sharpness [11]. The challenge lies in identifying a compromising combination of tool geometry and thermo-mechanical properties—such as the tool substrate and, if applicable, its coating—that can deliver optimal performance for each specific scenario. This requires a careful balance, as the tool must withstand the thermal and mechanical stresses of the machining process while maintaining efficiency and durability. The goal is to tailor the tool design to the specific material and cutting conditions, thereby maximizing its effectiveness and lifespan in challenging environments [3].

Figure 2.2 shows different cutting tool materials and it can be seen that the material with the highest toughness is HSS, however this family of materials is not appropriate to machine Inconel 718, as it has a very low hardness which would result in rapid tool wear [12]. On the other hand, diamond is very reactive with nickel, so diamond tools are not a suitable candidate either. PCBN can be used in the milling of Inconel 718, but typically for finishing operations given the relatively lower toughness and high production costs, so the two best candidates for this type of operation are carbide and ceramic [12].

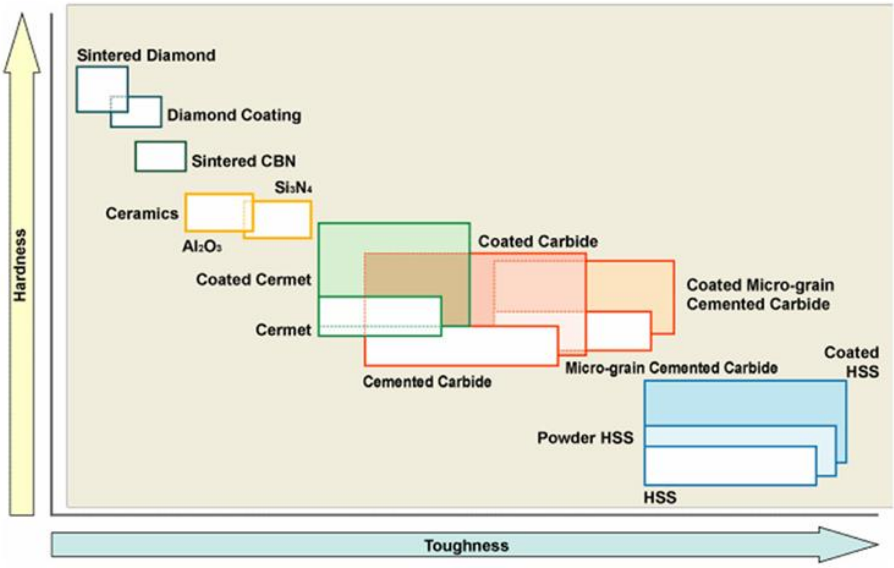

Figure 2.2: Hardness and toughness of different cutting tool materials [12].

Cemented carbide tools can be coated to increase resistance to abrasive wear, adhesion and diffusion, as well as to reduce friction (which lowers the temperatures involved in chip formation) and improve production quality. Examples of common coatings can be TiC, TiN, TiAlN, Al_2O_3, among others, applied by PVD or CVD, in single or multiple layers [12]. Nevertheless, carbide tools can only maintain appropriate mechanical strength up to half of the ceramic temperature spectrum (approximately 600°C) [13], which is insufficient to promote significant thermal softening of Inconel 718.

Ceramics, where SiAlON is located, at the intersection of Al2O3 and Si3N4, have lower toughness than carbides, which makes them less resistant to thermal shock [14]. However, they can operate at higher cutting speeds (3 to 10 times higher when compared to carbides [12]) due to their high resistance to temperatures, as well as improving feed rate values, which makes them more productive when machining. Ceramic tools are chemically more stable, resulting in less interaction with the machined material, which reduces the occurrence of diffusion wear mechanisms [13]. In addition, as ceramic tools have some resistance to adhesion and a low coefficient of friction, they can be used to reduce adhesive wear and material adhesion to the tools' surface, thus reducing the occurrence of BUE and other adhesive phenomena [13].

The cutting tool geometry can, as well, have a detrimental effect on the cutting operation. Milling can be carried out using inserts or with solid milling tools. Inserts are typically used in larger tools, commonly used for roughing operations and solid milling tools are typically smaller [15] commonly used for roughing or semi-finishing operations or the machining of small geometric features. Solid milling tools also offer greater dimensional accuracy, since they do not require calibration like inserts, in addition, they can have alternative geometries to traditional ones.

Figure 2.3 shows a 4-tooth solid milling tool, showing the different parameters used to characterize the geometry of these cutting tools. The parameters identified in Figure 2.3 include λ_s, which is the tool cutting edge inclination, also referred as helix angle, γ_o, which is the tool orthogonal rake angle, and α_{o1}, which is the tool orthogonal clearance angle.

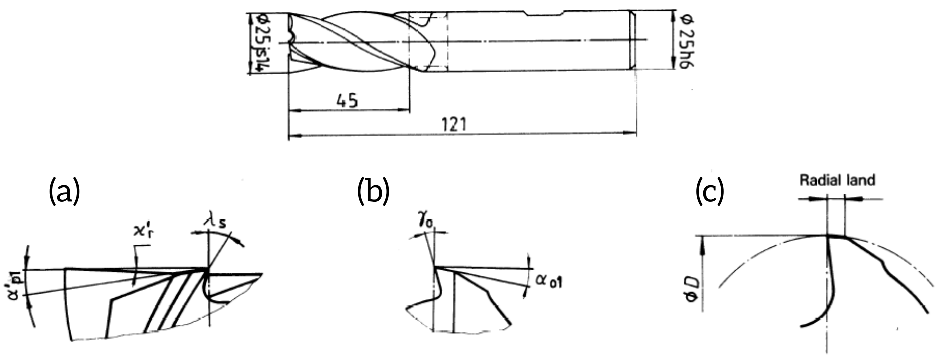

Figure 2.3: Geometry of solid milling tools and their relevant angles and features: (a) cutting edge inclination; (b) helix angle and (c) radial land, adapted from ISO 8688.

One of the most researched topics deals with improving the productivity of Inconel 718 machining through changes to the geometry of the cutting tools [3]. Tool angles greatly influence the cutting forces that will be generated. Negative rake angles lead to higher cutting forces, as well as higher temperatures in the cutting region and greater deformation of the workpiece's microstructure [16]. When the rake angle is negative, there is a larger contact area between the chip and the tool, thus increasing the friction between the surfaces. Similarly, positive angles help reduce generated cutting forces, temperatures and damage to the machined surface. Sharper cutting edges lead to lower cutting forces, but at the same time contribute to lower impact resistance [3]. Celaya et al. [17] suggest the use of rounded edges and smaller rake and clearance angles, to mitigate problems associated with this. Some authors, as Thakur and Gangopadhyay [18], suggest the creation of chamfers, as well as the creation of textured faces, with a view on increasing tool life [3]. The inclusion of textures on the rake and flank faces is referenced, especially when cutting fluids are used, to increase the rate of heat dissipation by the tool, increasing the tool's surface area. It also promotes lower friction in the tool-workpiece interface.

2.4 SiAlON as a cutting tool material

Among the ceramic materials, the two most relevant for the manufacturing of cutting tools are alumina (Al_2O_3) and silicon nitride (Si_3N_4), the latter include SiAlONs, which result from the dissolution of Al and O in the Si_3N_4 matrix [19]. However, ceramics can also be made of zirconia hardened with, for instance, alumina or a mixture of ceramics and can also be whiskers reinforced [19]. SiAlON has the advantage over silicon nitride of being less viscous, which makes it easier to densify, and allows dry machining even at high cutting speeds [20-22]. SiAlON is mainly composed by two phases: β-sialon, responsible for the toughness of the material, and α-sialon, responsible for the hardness [23].

The wear resistance of ceramic materials depends essentially on the compromise found between toughness and hardness, i.e. between the α and β phases [22]. An increase in toughness will invariably lead to a decrease in hardness. However, one way of achieving better mechanical properties is by refining the grain size of ceramics or reducing their glass phase, thus achieving better wear resistance [22].

Figure 2.4 shows the microstructure of a SiAlON, where it is possible to distinguish the α-phase, in grey, the β-phase, in black, and the inter-granular phase (in white). The α-phase usually has equiaxed grains, while the β-phase has a more elongated shape, with a ratio of 4:10 [24]. With an increase in the percentage of α-phase present the hardness of the ceramic increases too, as well as, the material's resistance to oxidation and the resistance to thermal shock [24]. It is also possible to add particles other than Si_3N_4 (e.g. WC, $MoSi_2$ and Ti(C,N)) to SiAlON ceramics in order to increase their mechanical properties [25].

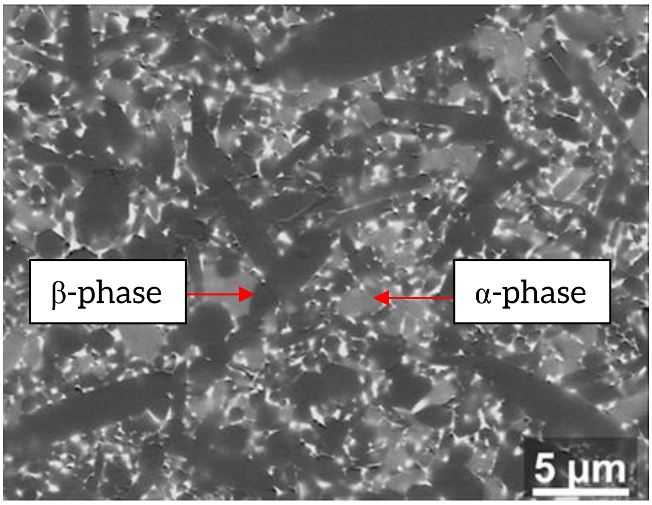

Figure 2.4: Microstructure of a SiAlON with 70% β-phase [26].

2.5 Wear and wear mechanisms

One of the most important aspects of studying cutting tools is understanding the wear and wear mechanisms that occur during cutting processes, trying to understand their causes, and how to minimize it. There are various tool wear mechanisms, such as adhesion, oxidation, abrasion, debonding, diffusion [27]. SiAlON cutting tools mostly show adhesive wear, diffusion wear and oxidation mechanisms [15, 28] during machining operations. However, these wear mechanisms do not occur separately on the tools, and the type of wear they exhibit is the result of a combination of several mechanisms [27]. Cutting tool wear can be of various types and, when it comes to machining superalloys, the most common forms are: flank wear, nose wear, notch wear, crater wear, BUE and edge chipping [22, 27-29].

Ezugwu et al. [29] report the occurrence of notching, chipping and flank wear on ceramic tools when machining nickel alloys at various cutting speeds, with adhesion mechanisms being the main culprit. The fact that high cutting temperatures are generated and the workpiece material softens leads to the formation of BUE, by cold-welding [28]. On the other hand, high temperatures also encourage oxidation reactions between the metal and atmospheric oxygen [27] and chemical reactions between the tool and the workpiece material, leading to diffusion of atoms between the contacting surfaces [22].

Through diffusion wear, the ceramic tool suffers a decrease in mechanical properties becoming more susceptible to mechanical impact, which can lead to the initiation of micro-cracks. The appearance of layers of oxidized material, which has a different coefficient of thermal expansion than that of the tool substrate [30], as well as the adhesion of material from the workpiece, favors the progression of these micro-cracks, leading to the formation of wear craters.

The abrasive wear mechanism is also frequently found in the machining of Inconel 718, due to the existence of carbides in the material's constitution, but also because, due to its high hardness, burr formation occurs during cutting operations. The existing burr from previous cutting operations will generally lead to an increase in abrasive wear [27].

Because it is one of the most common types of wear in superalloy machining operations, flank wear, VB, is used as a tool-life criterion. ISO 8688-2 specifies two recommended values to be used as end-of-life criteria for a solid milling tool. For uniform wear across all teeth, an average value of 0.3 mm is recommended, while for localized wear on a single tooth, a maximum value of 0.5 mm is suggested.

3 State of the Art

The following is a summary of previous studies on the subject. Some articles are presented on studies carried out in the field of machining with ceramic cutting tools. Regarding the studies presentation, whenever the studied material is not Inconel 718, a mention will be made.

Zheng and Zhao [31] carried out studies on up-milling processes with ceramic inserts, analysing the cutting forces involved in the process, as well as the temperatures, which they recorded using a thermographic camera, VB and the roughness of the machined surface and used different cutting speeds and two different a_e values, 12 and 19 mm, in the study. The authors found that the cutting forces are cyclical, with the component in the axial direction always showing the highest values. Up to cutting speeds of 1500 m/min, there is a gradual reduction in the resultant forces as the speed increases, which can be attributed to the thermal softening that occurs in Inconel 718, due to high generated cutting temperature. At low cutting speeds, the most significant failure mechanism was mechanical shock (impact), since temperatures are also low, and the tool is more fragile. At speeds above 1500 m/min, thermal stress plays a very important role, with the tool showing less VB. These tests show that wear occurs mainly on the cutting edge, but less on the rake face. When chipping occurs, the cutting edge undergoes a change in geometry and the solid milling tool can continue to cut, albeit without guaranteeing the dimensional accuracy of the process. Even so, this reshape capacity is not present at cutting speeds above 1600 m/min. The authors found abrasive and adhesive wear and the lowest values of roughness of machined surfaces were recorded for intermediate values of cutting speed, that also exhibit lower cutting forces, which may indicate that with lower cutting forces, the process has less associated vibrations.

Guo et al. [23] carried out milling tests with spark plasma sintered α/β-SiAlON inserts (one with 10% α-phase and the other with 40%), as well as with commercial inserts. The tool holder had an effective cutting diameter of 50.3 mm and an a_p value of 37 mm was chosen for down-milling operations. They first conducted several tests with different combinations of v_c, f_z and a_p concluding that the best machining parameters would be a v_c of 800 m/min, f_z of 0.12 mm/tooth and a_p of 1.5 mm. With these cutting parameters, they carried out experimental tests to compare the different tools. The authors concluded that the insert with the highest percentage of α-phase in its composition was the one with the best cutting performance; however, it showed flaking of the rake face and chipping of the cutting edge, which the researchers consider to be a result of its lower fracture toughness. The predominant wear mechanism found by the authors was adhesive wear, in all tools. They found that the adhesion of material was responsible for the removal of material from the tool and that this fracture surface was subsequently covered by new material that adhered to it.

Molaiekiya et al. [32] studied the impact of v_c and f_z machining parameters on generated cutting forces, temperatures and wear when up-milling with SiAlON inserts. They used inserts in a tool holder with an effective cutting diameter of 63.5 mm, with a_e of 34.5 mm and a_p of 1 mm and tested various v_c between 500 and 1300 m/min and f_z between 0.02 and 0.06 mm/tooth. To complement the experimental tests, they developed a numerical simulation model, applying a Lagrangian approach combined with adaptive remeshing capabilities. For the constitutive model they used the power law to describe strain hardening and rate sensitivity and a Coulomb's law for friction. For the lowest v_c, they found considerable chipping, but this decreased at intermediate v_c and increased again at 1300 m/min, showing considerable BUE formation at this cutting speed. Through numerical simulation, they obtained maximum cutting temperatures of 1300°C, with this value remaining stable for the different v_c studied. The authors found adhesive wear and abrasion wear as the dominant wear mechanisms and verified that the cutting forces were lower at a v_c of 900 m/min, which they justify not only by the softening of the Inconel 718 due to the dissolution of the carbides present, but also by the fact that at higher temperatures the metal alloy has greater thermal conductivity. The v_c value they used to carry out the tests with varying f_z was 900 m/min. The lowest wear was achieved on the tools machined with an f_z of 0.04 mm/tooth, and the numerical simulation showed that increasing the f_z contributes to greater heat distribution, as shown in Figure 3.1.

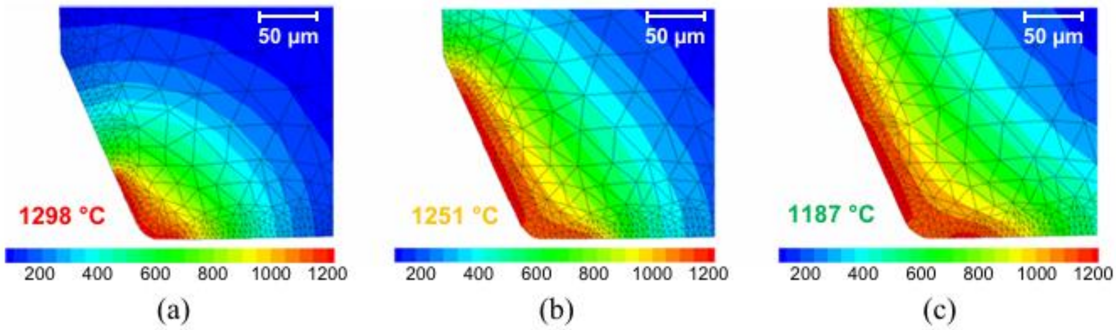

Figure 3.1: Temperature profile at different f_z obtained by numerical simulation by Molaiekiya et al.: (a) f_z=0.02mm/tooth, (b) f_z=0.04mm/tooth and (c) f_z=0.06mm/tooth [32].

Danh et al. [33] carried out milling tests on titanium alloys (Ti_6Al_4V) with SiAlON solid milling tools to open slots with the aim of studying sustained tool wear. Solid milling tools had a diameter of 8 mm and 4 teeth, these were used with a v_c of 250 m/min, f_z of 0.05 mm/tooth and a_p of 0.5 mm. The researchers observed that the tools started showing chipping marks for short cutting lengths and then, when cutting length increases, they found severe adhesion, including on the tool's substrate grinding marks (originating from grinding processes associated with tool production). This adhesive wear created several craters on the flank of the tool. They found also diffusion wear on the rake face and the flank face. Tool wear is most noticeable in the vicinity of the top cutting edges, since the a_p value is relatively low and the greatest wear was found on the rake face. The researchers concluded that high temperature promotes workpiece material adhesion to the tools' surface, as well as promoting diffusion phenomena. This leads to the formation of separate microcracks which then propagate and meet, resulting in the formation of craters, eventually causing tool catastrophic failure.

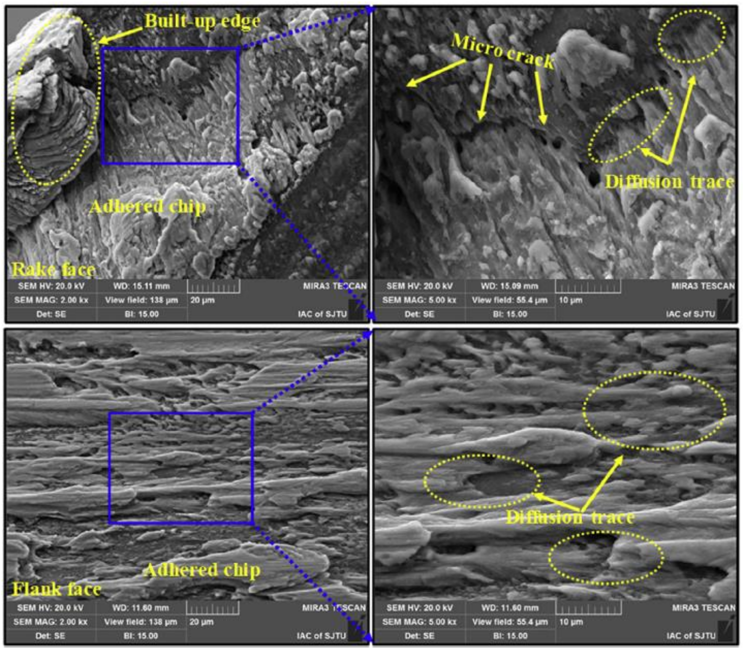

Figure 3.2: Wear mechanisms found on rake face (top) and flank face (bottom) by Huang et al. [34].

Also, Huang et al. [34] carried out milling tests with SiAlON solid milling tools, machining FGH96 nickel superalloy to study wear and cutting forces. The used cutting tools had a diameter of 10 mm and 4 teeth, using as fixed parameters an f_z of 0.04 mm/tooth, a_e of 0.5 mm and a_p of 4 mm, testing two cutting speed values: 255 m/min and 315 m/min. As the VB increased, the authors found that there was an increase in the contact area between the tool and the workpiece. An increase in cutting force values was also registered, with F_x (in the cutting direction) having the higher value, an increase in cutting temperature was registered too. Regarding wear mechanisms, they found that chipping or cratering occurred first and then, in the craters left by this, adhesion of the metal alloy occurred, resulting in the appearance of BUE. Figure 3.2 shows the various wear mechanisms found, in addition to adhesion, BUE, micro-cracks and diffusion wear marks can be seen. The fractures the authors found were brittle and, as the previous authors have identified [33], result from the propagation of different microcracks, that are later united. However, the wear on the rake face was less severe than the wear sustained by the tools' flanks. As tool wear increased, the machined surface showed greater surface roughness, particularly in the cutting direction.

In the study of wear mechanisms on milling operations performed with ceramic solid milling tools, Zimmermann et al. [15] conducted experimental tests with tools with a diameter of 8 mm and 4 cutting teeth, using a cutting speed of 503 m/min, a_e of 8 mm and one of two combinations of a_p and f_z: a_p of 0.4 mm with f_z of 0.15 mm/tooth or a_p of 0.24 mm with f_z of 0.08 mm/tooth. When comparing productivity with carbide tools, the ceramic solid milling tools showed an increase in the theoretical material removal rate and a decrease on the working time. The authors found evidence of chipping on the ceramic tools which contributed to a decrease in tool dimensions (tool geometry alteration), leading to the appearance of BUE in this "empty" area. However, the researchers report that the study of wear evolution was compromised by the occurrence of BUE, proving that adhesive wear and material adhesion is the dominant wear mechanism.

Also, Çelik et al. [26] studied the use of solid milling tools made of β-SiAlON to characterize their wear behaviour. The solid milling tools had a diameter of 12 mm and 6 teeth, furthermore, the tests were carried out with an a_e of 0.635 mm, a_p of 9.652 mm, f_z of 0.18 mm/rev and v_c of 585 m/min, specifically to ensure that temperatures at which the literature indicates that nickel superalloy begins to soften. There was adhesive wear on the rake and flank face, being identified by the authors as the main wear mechanism. The researchers also report the existence of a diffusion wear mechanism between the tool's flank and the workpiece, with the formation of a fragile layer that has several microcracks that propagate on the interface between the ceramic and a layer of oxides. Craters were also registered in the cutting tools.

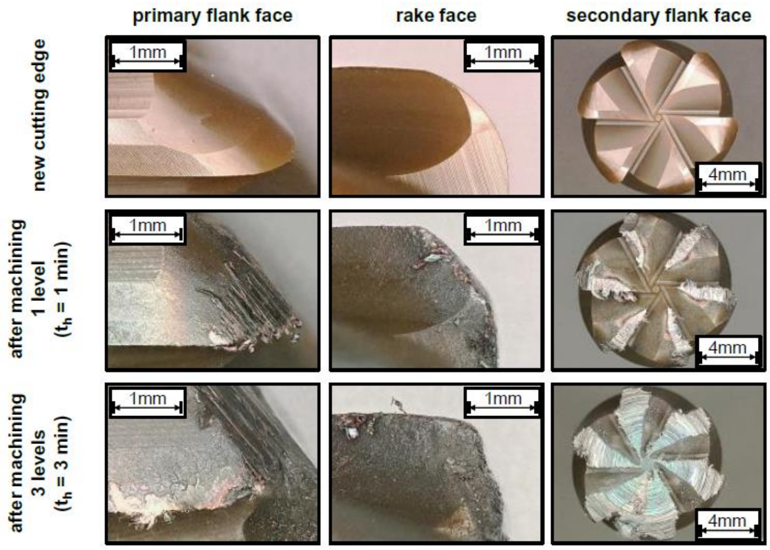

Figure 3.3: Wear on the rake face and flank face on new cutting edges (top), after 1min of cutting (middle) and after 3min of cutting (bottom) [19]

Finkeldei et al. [19], in turn, carried out studies using ceramic solid milling tools (silicon nitride) in end milling processes, opting for a linear milling strategy, to study cutting forces, wear mechanisms and the machined surface roughness. They used a 10 mm diameter cutting tool with 4 teeth and applied a v_c of 628 m/min, a f_z of 0.035 mm/tooth and an a_p of 1 mm as machining parameters. A cutting force of 28.8 N was recorded during the milling process, and as lower cutting forces are obtained, there is also less tool wear, mainly abrasive wear and changes in the cutting-edge geometry are registered, as can be seen in Figure 3.3.

However, there was a significant change in the microstructure of the machined surface due to the high cutting speeds. The grain is anisotropically deformed, but this layer has a thickness of 50 to 75 μm and can be removed in a finishing process with a maximum depth of 0.1 mm.

Ma et al. [13] also carried out studies using SiAlON solid milling tools in side-milling operations, focusing the study on generated cutting forces. The authors opted for an up-milling strategy to reduce the impact suffered by the cutting tool as it enters the workpiece material, and thus prevent premature fracture of the tool. The solid milling tools used had a diameter of 10 mm, 6 teeth and rake angle and relief angle of -5° and 25°, respectively. The a_p value was 5 mm and the a_e value was 0.5 mm. The v_c tested were 200, 275 and 350 m/min, with f_z of 0.08, 0.10 and 0.12 mm/tooth, in a total of 9 combinations of these two variables. It was found that with an increase in f_z and in v_c, the cutting forces also increased when using the SiAlON tools. The authors point to the occurrence of BUE with the increase in cutting temperatures as a possible cause of this. In the cutting direction it is possible to find small portions of chip material that has adhered to the new surface, and, in the a_p direction, notch undulations appear, which the authors attribute to tool wear. There is a VB of 0.53 mm on the SiAlON tools and craters can be seen in the areas where material adhesion occurs.

Zimmermann et al. [6] carried out studies to determine the influence of the wear mechanism on the machined surface. In their tests, they used solid milling tools with a diameter of 8 mm and 4 teeth and a v_c of 504 m/min and a_e of 8 mm (since they made slots within the material to be machined). The variables studied were a_p, whose values were 0.24 mm and 0.36 mm, and the f_z with values of 0.08 mm/tooth and 0.16 mm/tooth, with 4 combinations of these variables. All the tests were carried out with a cooling strategy: using pressurized air at 0.5 MPa. They found mainly BUE and chipping of the cutting edge, with the solid milling tool that operated with f_z of 0.16 mm/tooth and a_p of 0.36 mm exhibiting more wear, major changes in cutting edge geometry and severe flank wear due to abrasion. Also, the cutting forces recorded were greater for this combination of parameters, with an increase in cutting forces over the lifespan of the tool. Similarly, the temperatures measured on the workpiece also increased along the machining tests, reaching a difference of 100 °C between the temperatures recorded at the start of machining and those recorded at the end of tool life (after machining a cutting length of 10 m). Changes in the microstructure of Inconel 718 were studied and white layers were found, as can be seen in Figure 3.4, where there are no defined grain boundaries, with a maximum thickness about 5 μm. Immediately below this layer, a layer appears where grain boundaries exist but are still difficult to visualize. This layer has a greater thickness for higher cutting parameters and down-milling operations. A third layer was found where it is already possible to clearly define the grain boundaries and where they are oriented in the cutting direction, standing out from the rest of the material inside the workpiece. For down-milling operations, the thickness of this layer is greater.

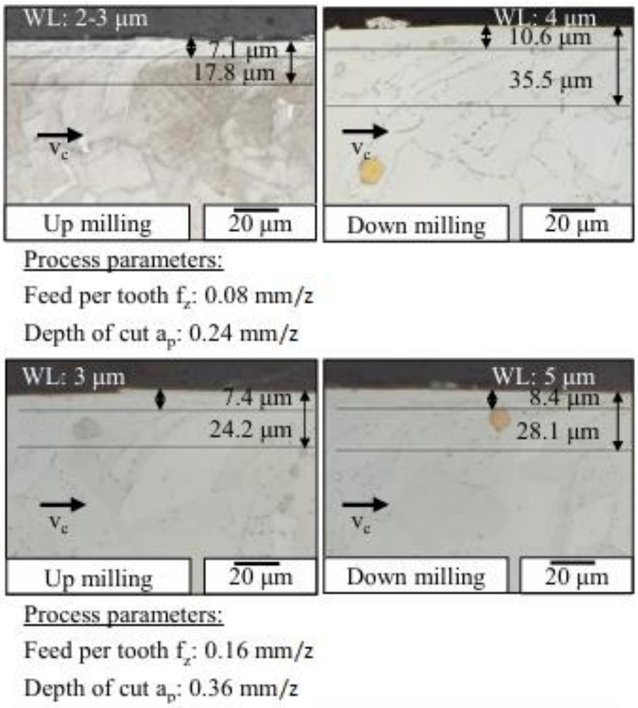

Figure 3.4: Microstructure of Inconel 718 after up-milling (left) and down-milling (right): top f_z=0.08mm/tooth and a_p=0.24mm and bottom f_z=0.16mm/tooth and a_p=0.36mm [6].

Parenti et al. [35] studied SiAlON solid milling tools with a diameter of 12 mm, 6 cutting edges, a helix angle of 35°, a radial rake angle of -5°, an axial rake angle of 2° and a cutting-edge radius of 10 µm. They used an f_z of 0.02 mm/tooth, a_e of 7.25 mm and a_p of 0.5 mm and studied v_c of 550 and 650 m/min, with an up-milling and down-milling strategy, applying a ramping strategy at the tool's entry into the workpiece to minimize initial impact. The authors found adhesive wear, with BUE formation and evidence of cutting-edge re-sharpening in all tests. The analysed adhered chips were oxidized and some of the tool's teeth presented fractures. The researchers found more damage on the solid milling tools that operated in down-milling, but the cutting forces were higher in up-milling operations compared to the former. This was registered, as well, for a vc of 650 m/min, compared to those recorded for a vc of 550 m/min. Lower v_c led to the appearance of more pronounced oxidation layers and poorer surface finishes.

Li et al. [36] carried out experimental tests with SiAlON solid milling tools with 4 teeth, a diameter of 12 mm, a helix angle of 30° and a cutting-edge radius of 1.5 mm. The authors opted for a down-milling strategy, with a v_c of 500 m/min, a_e of 0.5 mm, a_p of 3 mm and tested f_z of 0.04 and 0.06 mm/tooth. The higher value of f_z led to greater cutting forces, with the component in direction perpendicular to the feed being the component with the greatest amplitude. Higher f_z also leads to greater machined material adhesion on the flank face, forming shear bands. The others wear mechanisms identified were abrasion wear and diffusion wear. On the rake face, there was less evidences of adhered material, but the main wear mechanism was adhesive wear, furthermore, cracks and chipping were also found.

Sun et al. [28] studied the down-milling performance of ceramic solid milling tools in order to analyse generated cutting forces, temperatures, wear and surface quality. They used tools with a diameter of 12 mm, 6 teeth, cutting-edge radius of 2 mm, helix angle of 45°, rake angle of -15° and clearance angle of 15°. They performed a linear strategy on a block instrumented with a k-type thermocouple, as shown in Figure 3.5, coated with a high temperature conductive paste, with a v_c of 400 m/min, f_z of 0.04 mm/tooth, a_p of 4 mm and a_e of 0.8 mm. The highest force recorded was in the direction perpendicular to the feed and the lowest force was in the axial direction, achieving a maximum resultant force with ceramic tools that was 13.5% lower than that recorded with cemented carbide tools. Ceramic tools were more efficient, achieving a material removal rate of 135.83 mm^3/s (1.5 times better than cemented carbides) and lower surface roughness. As VB increases, surface roughness increases, as do temperatures. Although temperatures follow a trend of increasing rapidly at first and then gradually decreasing. On both the flank face and the rake face, the authors found adhesive wear, BUE formation and chipping, in addition to cracking and diffusion wear on the flank face.

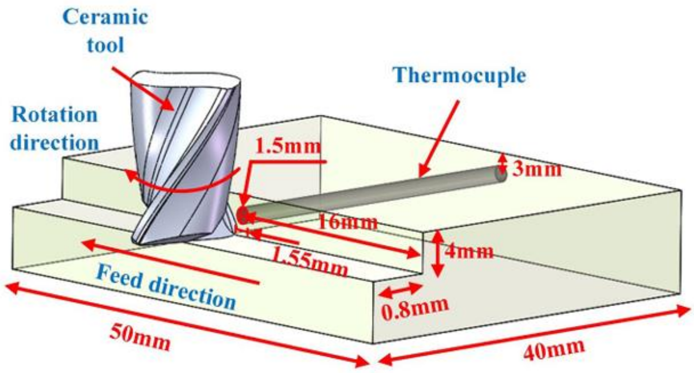

Figure 3.5: Scheme of the experimental setup for measuring temperatures used by Sun et al. [28].

Holmberg et al [37] carried out tests to study the differences between down-milling and up-milling strategies, by opening 16 mm wide slots in the workpiece. The authors studied machined surface roughness, workpiece grain deformation and residual surface stresses, as well as cutting tool wear. They used inserts in a holder with a diameter of 25 mm, applying v_c of 800 m/min, a f_z of 0.07 mm/tooth and a_p of 1 mm. The authors found that surfaces machined with new cutting edges show lower surface roughness compared to surfaces machined with worn cutting edges, but, in both cases, the up-milling strategy always showed greater surface roughness when compared to the down-milling strategy. All the samples showed grain boundary deformation located in a well-identified layer. The researchers concluded that, when creating slots in the workpiece there were transition zones between the up and down-milling zones, which showed higher residual stresses. They suggest that slotting should be avoided with ceramic solid milling tools. Both the up and down-milling strategies show a similar distribution of stresses, although in the case of new inserts, they show greater wear when used in a down-milling strategy. On the other hand, in the case of inserts with some use, the greatest wear was recorded in up-milling operations.

For this reason, the authors suggest implementing an up-milling strategy until the cutting-edge is worn, then switching to a down-milling strategy, which will produce less deformation in the workpiece.

Hadi et al. [38] also carried out a comparative study between up and down-milling operations using inserts, studying wear and chip formation. They used 10 mm diameter tungsten carbide inserts coated with PVD TiAlN/AlCrN, analysing the evolution of wear as 60 mm lengths were machined. The authors also varied v_c, f_z and a_p. The authors observed that in up-milling operations, wear was greater and began to be evident at the end of one pass (while in down-milling operations wear was recorded after the 20th pass) and found that a larger hardened layer is created on the workpiece's surface. Tool wear in these operations was found to be directly proportional to the a_p, as well as to f_z. An increase in vc leads to an increase in wear, although there is no direct proportional relationship, according to the authors. The increase in wear is a result of the increase in abrasive and adhesive wear on the flank face. The wear seen in down-milling is lower for all the studied parameters and the machined surface quality is better. However, the impact on the tool is also greater, which can lead to chipping. The propagation of wear on the cutting tools' flank was much faster for the up-milling operations than the down-milling operations. In up-milling, the formed chips tend to have a saw tooth shape, whereas in down-milling, the chips tend to be discontinuous and serrated, as can be seen in Figure 3.6.

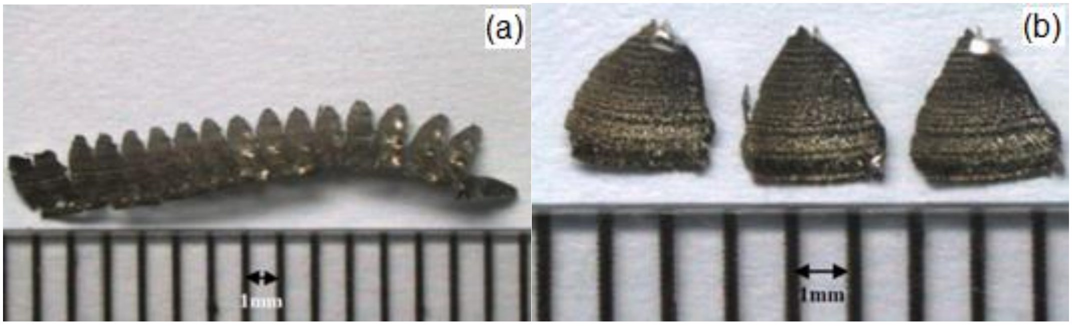

Figure 3.6: Chips formed in up-milling (a) and down-milling (b) operations [38].

Pitallà et Monno [39] studied the creation of a 2D simplification model for the milling of Ti-6Al-4V with the objective of estimating the process' temperatures. The DEFORM 2D software was used, applying the Johnson-Cook model as the constitutive model, the Cockcroft & Latham model as the damage model, and the shear constant model as the friction model. Figure 3.7 shows the definition of the tool geometry, defined as a rigid body, used by the authors, as well as the defined boundary conditions. Several simulations were conducted for different chip thicknesses to simulate up-milling, where the chip starts with the smallest thickness and increases to its maximum value. The cutting forces obtained from the numerical model were compared to those measured experimentally by the authors and served as the validation criterion for the numerical simulation. Compared to other models from different authors, this new model offers results closest to the experimental values.

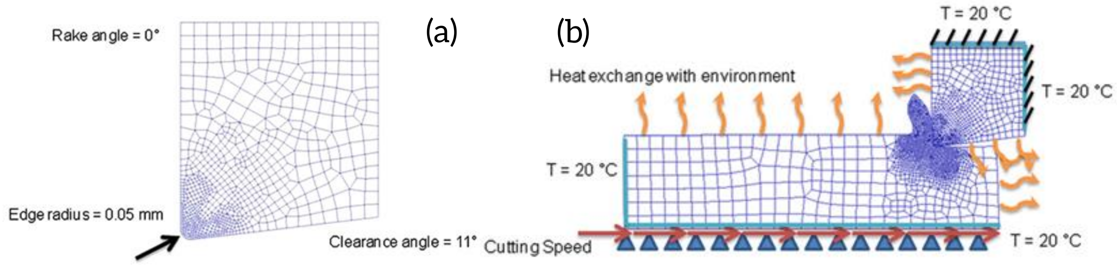

Figure 3.7: Representation of the tool geometry defined in the numerical model (a) and the applied boundary conditions (b) by Patallà and Monno [39].

4 Materials & Methods

4.1 Experimental setup

Experimental tests were carried out to study the performance of solid milling tools with different geometries and different chemical compositions in end milling Inconel 718. The aim was to gather information on generated cutting forces, torques, tool wear, temperatures and machined surface integrity. Two distinct milling path strategies were defined, linear and spiral and two types of milling modes were tested, up-milling and down-milling, using solid milling tools. Heat treated Inconel 718 (970°C for one hour, followed by cooling in water) was used. This heat treatment resulted in an alloy with grain size of 8 μm and hardness of 441 HBW. Table 1 shows the chemical composition of the used Inconel 718, which was measured using spark spectroscopy analysis.

Table 1: Inconel 718 chemical composition (mass wt.%).

Ni	Cr	Fe	Cb	Mo	Ti	Al	Co	Si	Mn	Cu	C
53.83	17.94	17.67	5.33	2.90	1.00	0.52	0.20	0.09	0.08	0.05	0.02

Solid milling tools with two different geometries were employed, varying on teeth number (4 and 6 teeth). All solid milling tools with 4 cutting edges were manufactured with the A substrate and all those with 6 were manufactured with the B substrate. Table 2 shows the percentage of α and β-phases for each of the tested substrates. Figure 4.1 and Figure 4.2 show the geometry of each cutting tool. Table 3 shows the geometric parameters of the used end-mills.

Table 2: Chemical composition of the different SiAlON substrates.

Substrate	α-phase (%)	β-phase (%)	Yttrium
A	25	69	6
B	31	61	8

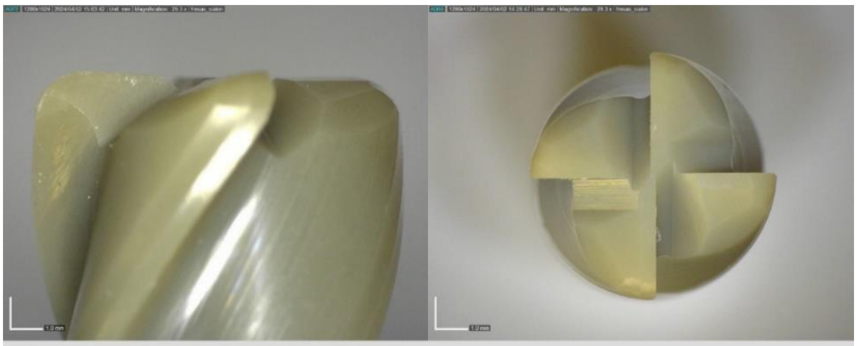

Figure 4.1: Solid milling tool geometry with 4 teeth (4Z).

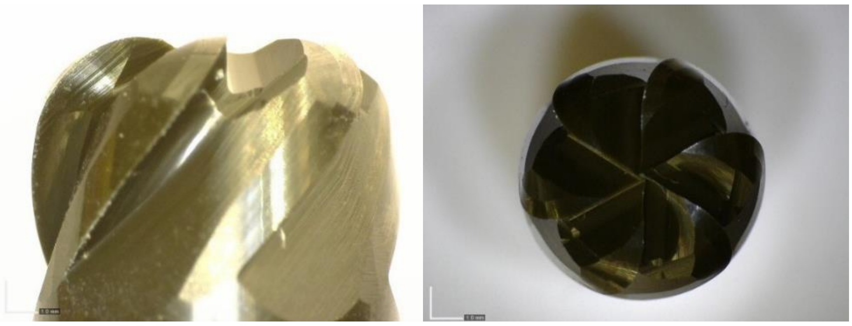

Figure 4.2: Solid milling tool geometry with 6 teeth (6Z).

Table 3: Geometry of the different solid milling tools used in the experimental tests.

Tool	4Z	6Z
Diameter (mm)	8	8
Rake Angle (°)	0	-3
Clearance Angle (°)	6.1	7
Helix Angle (°)	33	42

The Inconel 718 raw material sample, a rod with a diameter of 158 mm, was prepared differently for each milling path strategy (linear and spiral). For the linear strategy, an 8 mm thickness disc was cut from the 158 mm rod using EDM. This disk was posteriorly cut in half, producing two workpieces (two half-disks). One half of the disk is shown in Figure 4.3a, clamped on a vise to the milling center working table. The instrumented tests were carried out on a DMG Mori DMU 60 eVo CNC milling center with 5 axes and a maximum nominal angular speed of 18,000 rpm.

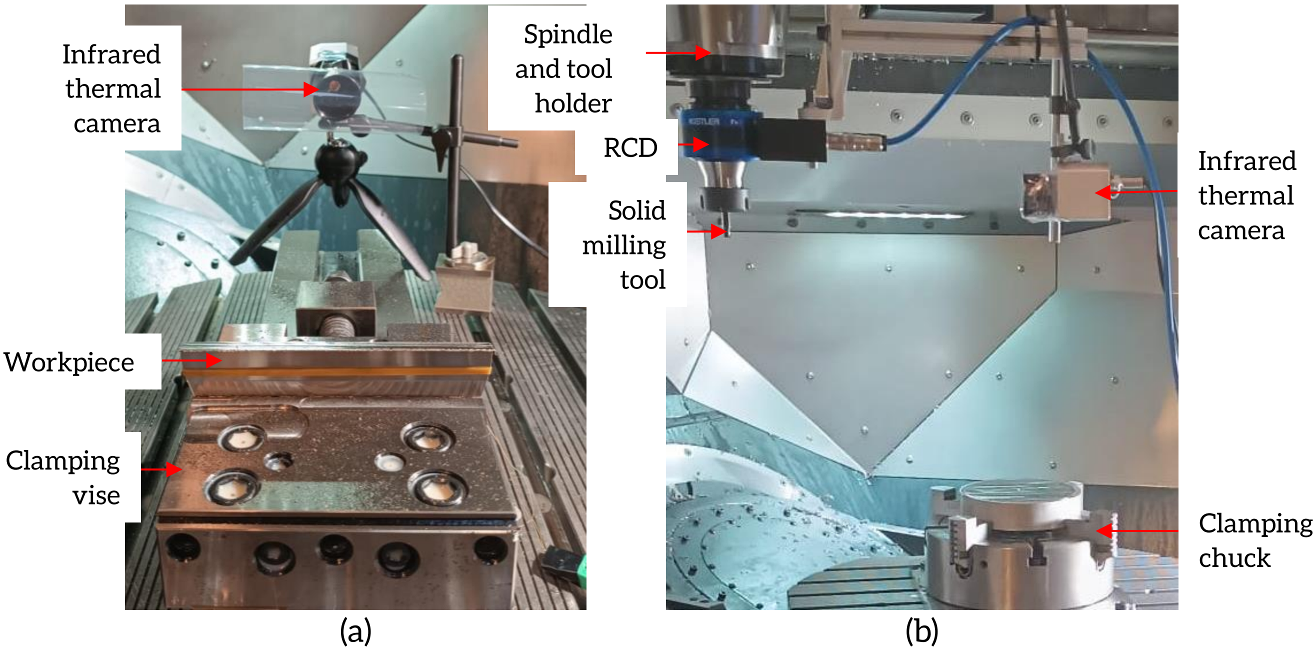

Figure 4.3: Setup for the linear strategy (a) and for the spiral strategy (b) experimental tests.

For the experimental tests with the spiral trajectory strategy, a cylinder with a height of 39 mm was used (with 158 mm in diameter), which was clamped as shown in Figure 4.3b. To collect data on the cutting forces in the three cartesian axes (F_x, F_y and F_z), F_a and the M_z, a Kistler model 9170 a Rotating cutting force dynamometer (RCD) was used in all conducted tests. The RCD was mounted directly on the CNC spindle, so that it could measure loads and torque on the tool (contrarily to load cell mounts on the machine working table), which made it possible to draw polar torque maps of the different teeth of each tool using the collected data. The generated data was then collected using Dynoware software, where it was pre-processed.

In addition, an infrared thermal camera was used to record cutting temperatures during the machining tests, the Optris model PI 400i, which allows the choice of one of four temperature ranges: [-20;100], [0;250], [150;900] and [200;1500] °C. In the tests carried out using the linear strategy, the camera was fixed to a support in the press and placed so that the workpiece's surface was in the image's frame, as can be seen in Figure 4.3a. Initially, the temperature range chosen was 0 to 250°C in order to capture its evolution in near-transient conditions, starting from room temperature. In the tests carried out with the spiral strategy the infrared thermal camera was mounted so that it moved synchronous with the spindle, as shown in Figure 4.3b, and, consequently, with the tool. In these tests, the temperature range chosen was 150 to 900°C in order to capture its evolution for longer cutting lengths. All temperature data was collected and processed using Optris PIX Connect software.

4.2 Cutting parameters

Three different sets of cutting parameters were employed in this study. Those configurations were selected based on the literature review, aiming at representing typical milling operations, for instance, (i) $a_p >> a_e$ for highly productive contouring and (ii) $a_p << a_e$ for slotting. The third combination uses intermediate values of these two parameters.

Table 4 provides a summary of the parameters used in the different experimental tests, as well as the milling strategy and mode used for each solid milling tool. In order to test contouring operations, an a_e value of 0.4 mm, which is 5% of the tool diameter, was chosen, while the a_p value used was 5 mm. In tests closer to slotting operations, the used a_e value was 40% of the solid milling tool's diameter, 3.2 mm, and the a_p value was 0.1 mm. In the third combination, the a_e chosen was 20% of the tool diameter, corresponding to an a_e of 1.6 mm. Of the articles studied in the literature review, the a_p value is between 0.24 mm and 5 mm. Previously, with tools of the same composition from the same supplier, some preliminary tests had been carried out in which this parameter was set at 0.5 mm and as this is a value used by many authors when conducting similar machining operations [23, 33, 35, 36], it was considered coherent to choose this value for the experimental tests.

The three sets of parameters were used in tests conducted with a spiral strategy using solid milling tools that had 6 cutting teeth (6Z) in down-milling mode. In this milling strategy, the goal is to achieve a longer cutting length without interruptions, thereby eliminating the number of tool entries and exits on the workpiece, therefore minimizing the impact experienced by the cutting tool.

For the linear milling strategy, only the intermediate combination of a_e and a_p was used with solid milling tools 4Z (4 cutting teeth) and 6Z, in both up-milling and down-milling modes. All other parameters remained constant throughout the experimental trials.

The literature review found very different v_c values, ranging from 60 m/min to 3000 m/min. Given the limitations of the used machining center (18,000 rpm maximum nominal rotational speed), the studied v_c, for a solid milling tool with the 8 mm diameter mentioned above, has a maximum possible value of 452.4 m/min (Equation 4).

Following the results obtained by various authors [13, 33, 34], v_c values below 200 m/min were discarded, leaving a possible range between 200 m/min and 450 m/min (approximately). However, the literature review shows that ceramic solid cutters perform better at higher cutting speeds. Given the scarcity of cutting tools available for the tests, only the highest value, 400 m/min, (the same v_c used by Sun et al. [28]), was chosen and it remained constant for all the conducted tests. For this v_c the machine's spindle will be set at 15,916 rpm.

The value chosen for the f_z parameter in the different analyzed studies is between 0.032 mm/tooth and 0.16 mm/tooth. The studies indicate that higher feed-per-tooth values lead to more satisfactory results as far as tool wear is concerned, although this is not always the case. The 0.08 mm f_z value is commonly found in various studies [6, 15, 28] and was the value chosen for the experimental tests.

Table 4: Summary of the parameters, strategy, and milling mode used for each tool in the practical tests.

<table>
<tr><th>Parameters set number</th><th>Milling tool code</th><th>ap/ae</th><th>Fixed Parameters</th><th>Strategy</th><th>Mode</th></tr>
<tr><td>1</td><td></td><td>a_p=5mm
a_e=0.4mm</td><td rowspan="7">v_c=400m/min
f_z=
0.08mm/tooth</td><td>Spiral</td><td>Down-milling</td></tr>
<tr><td>2</td><td></td><td rowspan="5">a_p =0.5mm
a_e =1.6mm</td><td>Spiral</td><td>Down-milling</td></tr>
<tr><td>3</td><td>UM4Z</td><td>Linear</td><td>Up-milling</td></tr>
<tr><td>4</td><td>DM4Z</td><td>Linear</td><td>Down-milling</td></tr>
<tr><td>5</td><td>UM6Z</td><td>Linear</td><td>Up-milling</td></tr>
<tr><td>6</td><td>DM6Z</td><td>Linear</td><td>Down-milling</td></tr>
<tr><td>7</td><td></td><td>a_p =0.1mm
a_e =3.2mm</td><td>Spiral</td><td>Down-milling</td></tr>
</table>

4.3 Data collection

4.3.1 Tool wear inspection

A digital microscope (Dino-Lite) was used to assess wear, through image capturing, as can be seen in Figure 4.4. All the milling cutters were analyzed, both from the side (primary cutting edges) and from the top (secondary cutting edges), before being used. In the tools that performed linear milling strategies (several tool entries and exits), images were taken at each pass of the tool through the workpiece (every 158 mm of cutting length). In the case of the solid milling tools used in the spiral strategy the solid milling tools were only photographed at the end of the operation. After photographing the cutting tools, these were measured using the ImageJ™ software.

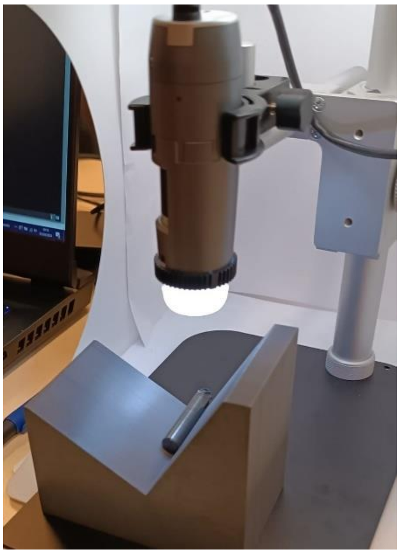

Figure 4.4: Dino-lite capture of a solid milling tool after a milling operation.

In addition to analyzing the photographs taken with the Dino-lite, the cutting tools were also analyzed by SEM after machining. This was done to better assess and characterize tool wear, carrying out EDS analyses as well.

4.3.2 Surface Integrity

In terms of surface integrity, machined surface roughness was assessed, furthermore, an analysis of the microstructure of cut samples was performed, duly prepared for this purpose.

To assess the roughness of the machined surface, R_a, R_z and R_{zmax} were measured using a Mitutoyo SJ-210 surface roughness tester. In the linear tests, the measurement was made at the end of 790 mm cutting length (5 linear passes of 158 mm each), i.e. the equivalent of one surface facing, while in the spiral tests the measurement was performed at the end of the proposed operation for each tool. The samples for microstructure analysis were taken after machining operations using the linear path strategy. After cutting, they were properly treated so that their microstructure could be analyzed.

The samples were subject to grinding operations using SiC paper with varying grits, following the section: 320, 600, 1000 and 4000 grit. Then the samples were polished with a diamond suspension with 1 μm average particle size and, posteriorly, with colloidal silica with 0.06 μm average particle size. After this preparation, the samples were electrolytically etched using a current voltage of 6V and a current of 1 A, in a 5% oxalic acid solution, for 1 s.

4.4 Simulation of the cutting process using the Finite Element Method

To transform the plastic properties of the Inconel 718 used in the experimental tests, the flow curves were defined using the Johnson-Cook (JC) model, as described in Equation 6. Static compression tests were conducted by Matos [40] to obtain the constants that make up the first term, which define the flow curve under ambient temperature and steady-state conditions. The data from the static compression tests, as well as the other constants used in the JC model, are presented in Table 5.

$$\bar{\sigma} = [A + B\varepsilon^{-n}]\left[1 + C\ln\left(\frac{\dot{\bar{\varepsilon}}}{\dot{\bar{\varepsilon}}_0}\right)\right]\left[1 - \left(\frac{T - T_{amb}}{T_f - T_{amb}}\right)^m\right]$$ *Equation 6*

Table 5: Constants used in the JC model for the numerical simulation.

Constant	Value
A	600
B	1200
C	0.0014
n	0.4
m	0.7
$\dot{\bar{\varepsilon}}_0$	1
T_{amb}	20
T_f	1430

Friction was modeled using a shear friction coefficient of 0.4, while the heat transfer coefficient was defined as 45 N/s/mm/°C. All other thermal properties of Inconel 718 were assigned according to the material defined in the library of the software used for creating the numerical simulation and are described in Table 6 and Figure 4.5.

Table 6: Thermal properties defined for the Inconel 718 used in the numerical simulation.

Property	Value
Emissivity	0.8
Mass density	8.19e-9 tonne/mm^3

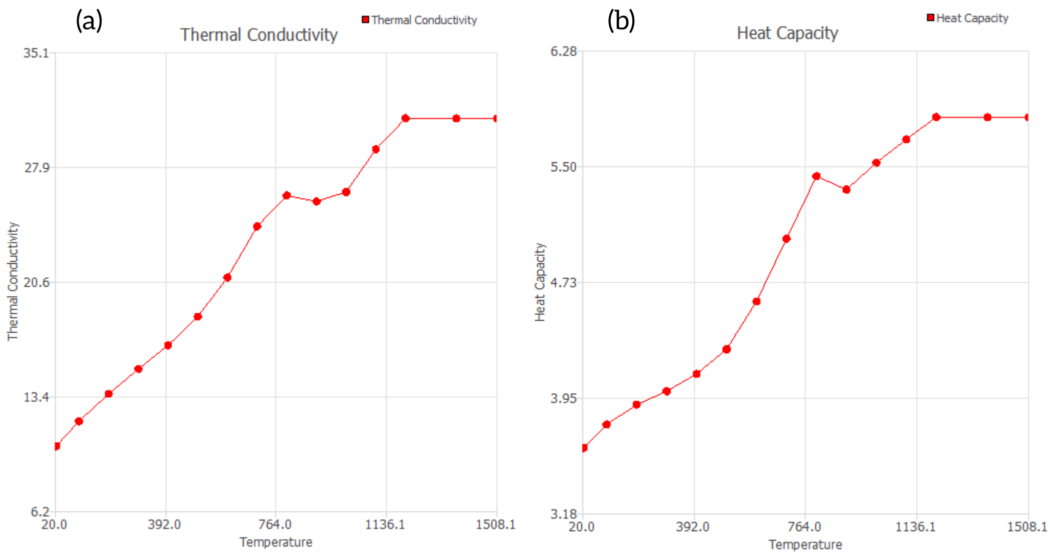

Figure 4.5: Thermal properties of Inconel 718 as a function of temperature: (a) Thermal conductivity and (b) Heat capacity.

The numerical simulation was performed using the DEFORM 2D software, which employs an implicit Lagrangian approach, and a 2D simplification of the cutting process carried out by one of the teeth of the solid milling tool in contact with the workpiece was made, as used by Pitallà and Monno [39], approximating the process to an orthogonal cutting process.

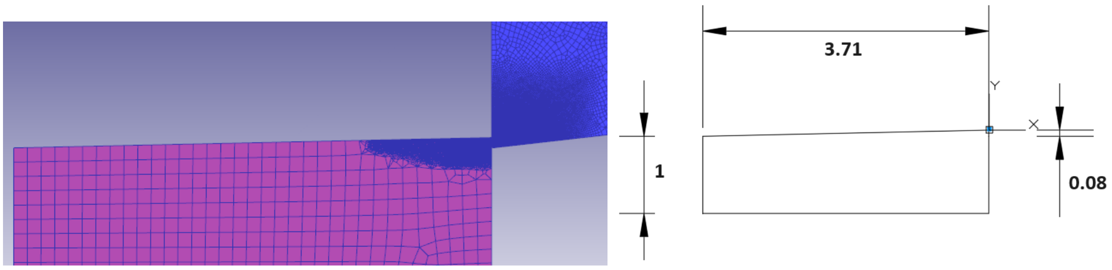

Figure 4.6: Geometry of the workpiece used in the 2D numerical model for representing the down-milling mode

Figure 4.6 shows the defined geometry for the workpiece used in the numerical simulation of the down-milling process. As previously shown, the surface that will be in contact with the cutting tool features a slope to simulate the variation in chip thickness throughout the process, starting with the maximum thickness (defined as 0.08 mm) and ending at a thickness close to zero. The length of the workpiece was calculated based on the rotation angle of the solid milling tool, corresponding to the passage of a single tooth, which represents the arc of the circumference defined by the cutting edge passing through the workpiece.

The workpiece was defined using the von Mises yield criterion (J2) with isotropic hardening, based on the flow curves, while the tool was defined as a rigid body. Table 7 presents the thermal properties applied for defining the Inconel 718 and SiAlON.

Table 7: Thermal properties defined for the SiAlON used in the numerical simulation.

Property	**Value**
Thermal Condutivity	20.5 N/s/mm/ºC
Vol. Heat capacity	1.45 N/mm^2/ºC
Mass density	3.3e-9 tonne/mm^3

5 Results and Discussion

5.1 Cutting Forces

In order to be able to analyze and compare the behavior of the different cutting forces (F_a, with its components F_c and F_{cn}, and F_z), a complete analysis on the measured cutting forces was carried out as to compare the different milling strategies (linear and spiral), modes (up- and down-milling) and tool geometries (4Z and 6Z).

Figure 5.1 shows a graphical representation of the type of data collected by the RCD for the active cutting force, F_a, for a cutting length of 158 mm on a UM4Z tool. The graph shows a dense data collection due to the chosen high acquisition rate (10 kHz). However, by selecting only a shorter time interval, it is possible to observe the load evolution for one complete rotation of the solid milling tool. The signal shows a sinusoidal shape, and the existence of 4 peaks is noticeable, corresponding to the passage of each tooth.

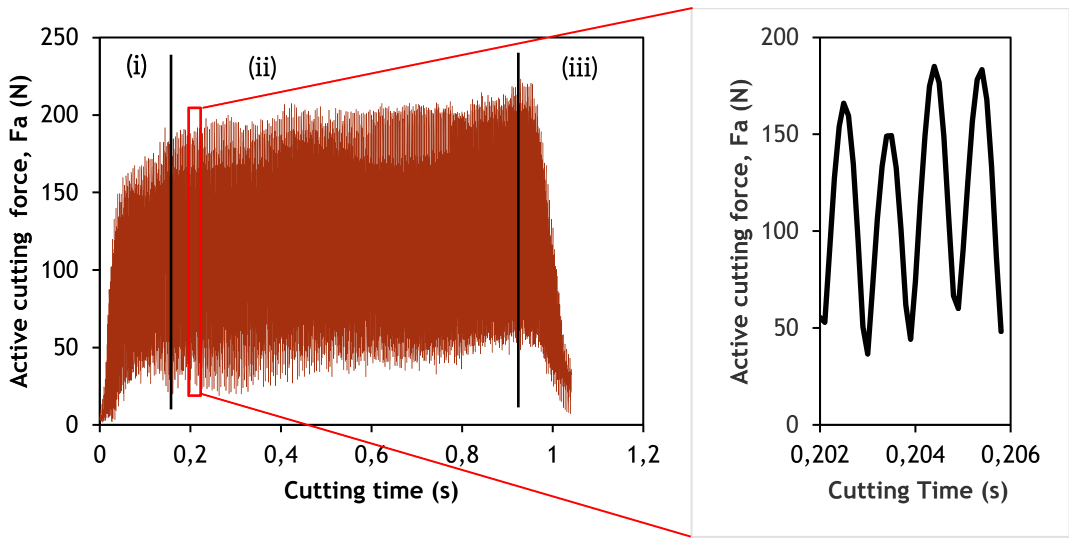

Figure 5.1: Graphical representation of the experimentally collected F_a and detail of a single rotation period of the tool.

Milling is a discontinuous cutting operation meaning that the cutting force signal will oscillate between maximum values, corresponding to the moments when the chip thickness is the largest, and minimum values, when chip thickness is null. It is interesting to note that for null chip thickness there is still force magnitude (approximately 50 N) which may be due to the passive force component (F_{cn}) that assumes non-zero values due to the bound contact promoted by friction and vibration.

It is noticed that the force signal, despite its oscillation, is composed of 3 main fases: a (i) transient force evolution, a (ii) steady state force plateau and (iii) a force decrease. One aim of the present analysis was to find a representative average value of the milling operation at its steady state. Several ways of finding this average value were tested. The first method was to calculate the average value of all the data collected for the F_a. The second method was to calculate the average value exclusively using data where the process was already in a stationary regime. Finally, the third method consisted of calculating the average of all active force maximum values within the steady state stage. Table 8 shows the values obtained for the three tested methods for calculating the average values of the F_a for the UM4Z solid milling tool. The first two tests showed that the impact of the data on the tool's entry and exit from the workpiece has negligible effect on the final result.

Table 8: Methods for calculating average active force value.

	Method 1	**Method 2**	**Method 3**
Method result (N)	117	119	172

When comparing the average Fa values with the average of the Fa maximum values, a clear difference is noticed. Due to its better representation of the Fa value at the maximum chip thickness, method 3 has been used to calculate all the maximum Fa average values presented in this section.

Figure 5.2 shows the graphical representation of the different cutting loads recorded for solid milling tools with 4 teeth, as well as the trend lines of their evolution. Each point on the graph corresponds to one pass, so the UM4Z solid milling tool made a total of 9 passes and the DM4Z solid milling tool made a total of 11. As the cutting length increases, all the cutting forces show a monotonic positive trend. This effect can be explained by tool wear. In fact, throughout the life of the tool, as wear increases, the cutting forces tend to show higher values, as the geometry of the cutting edges changes. Zimmermann et al. [6] have also found this increasing trend in their studies and point out the loss of cutting capacity (cutting edge deterioration) of the tools as the likely cause. On one hand, there is high adhesion of Inconel 718 to the tool's surface, not only because the material becomes more ductile when machined at high cutting speeds, but also because, given the geometry of the solid milling tool, it is difficult to evacuate the formed (and adhered) chips. On the other hand, in addition to material adhesion, chipping phenomena often occur, which may or may not be accompanied by reshaping of the cutting edge, but which in any case alters the cutting capacity of the tool.

All the changes in the geometry of the solid milling tool also result in a change in the F_{cn}, which can be seen to have a greater contribution to F_a when compared to the F_c component. The F_{cn} is responsible for the deflection imposed on the tool and an increase in this cutting force will result in an increase in vibration magnitude, which, in turn may increase the cutting forces involved in the cutting process.

When comparing the up-milling and down-milling cutting forces, it can be seen that in all sub-figures of Figure 5.2, the up-milling trend lines are always higher than the down-milling ones.

It can be noticed that down-milling operations are less demanding for the cutting tool's integrity than up-milling operations and, consequently, show lower energy consumption too. Holmberg et al. [37] and Hadi et al. [38] reached a comparable conclusion in their respective studies. From a point of view of smoothing impact/collision between the cutting tool and workpiece the up-milling strategy might seem more advantageous, given the zero-chip thickness cutting start.

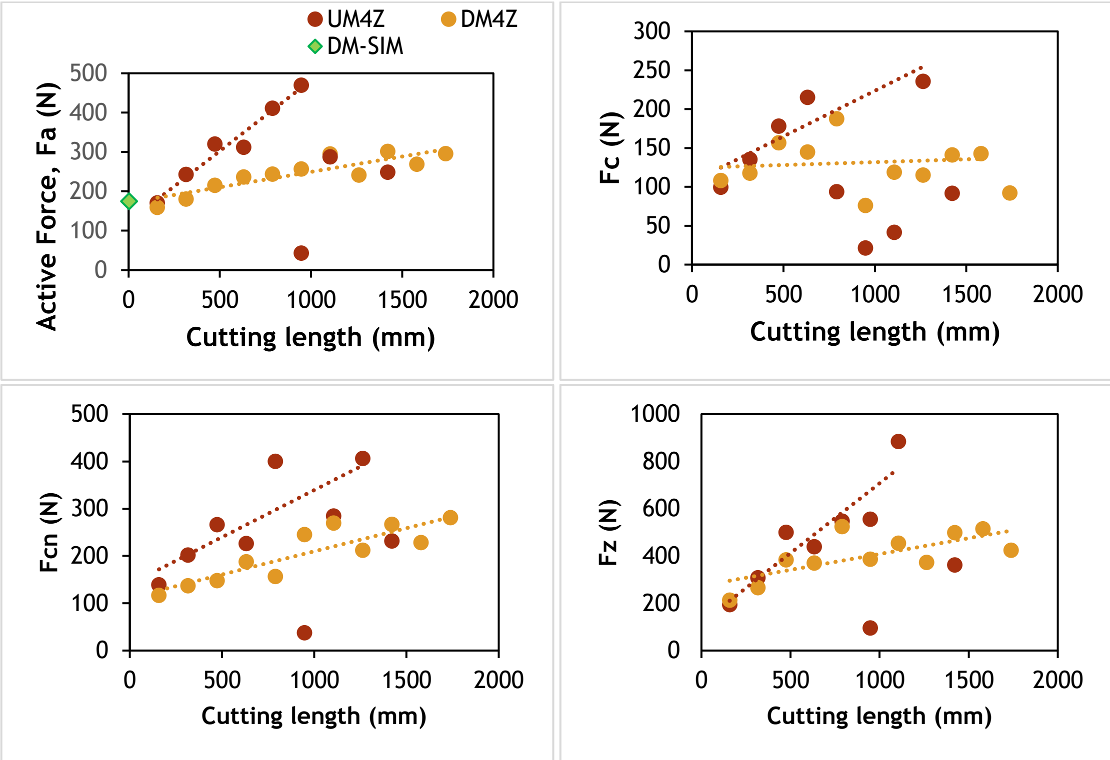

Figure 5.2: Graphical representation of the cutting forces for the UM4Z and DM4Z solid milling tools: F_a (top), F_c (middle left), F_{cn} (middle right) and F_z (bottom)

Although in up-milling operations the chip starts at a lower thickness, which might be seen as an advantage in terms of minimizing the magnitude of tool-workpiece impact, the larger amount of friction, especially between the flank face and the newly generated surface of the workpiece, leads to greater wear. Therefore, although the tested SiAlON tools have lower toughness than conventional solutions such as WC-Co, they still sufficiently withstand the discontinuous chip formation typical of down-milling conditions. It should also be noted that, in addition to presenting trend lines with smaller slopes, down-milling operations exhibit smaller deviations between the recorded data and the trend of the cutting forces, suggesting a more controlled cutting process. The F_c and F_z loads show experimental values outside (in the up-milling mode) of the identified cutting load increasing trend (for larger cutting length). The intense adhesion of the workpiece material to the tool and its subsequent removal during the cutting process may introduce a deviation in the forces recorded by the RCD, leading to the appearance of outliers, such as those found in Figure 5.2. This may be an additional indicator of the lack of process stability in up-milling, as adhered chip (as will be further seen in section 5.2) may unexpectedly release from the cutting tool, causing load fluctuation. In addition, although it can be said that down-milling is a better solution, it can be assumed, by analyzing this behavior of the components of F_a, that it may be necessary to revise either the geometry of the solid milling tools or the parameters in which this geometry is being applied, in order to optimize operations.

Figure 5.2. also allows for a comparison of the Fa value estimated using the finite element method with the values obtained experimentally, for both up-milling and down-milling modes, when considering the cutting length corresponding to the passage of only one cutting edge on the workpiece. Since the value estimated by the numerical model does not account for the tool wear, only cutting lengths very close to zero can be compared. When comparing the values recorded in the experimental tests with the estimated values for Fa (both in up-milling and down-milling), they are found to be similar, thus confirming that the developed numerical model model (definition of the uncut chip area, flow curve, friction conditions) adequately portray the behaviour of the materials involved in the cutting process. This also suggests the possible use of the developed numerical model to estimate additional variables, such as process temperature or contact pressures at the interface between the tool and the workpiece, to better understand the differences between the tribomechanical conditions in the two milling modes studied.

Figure 5.3 shows the graphical representation of the various cutting forces for the solid milling tools with 6 cutting edges. The UM6Z solid milling tool made a total of 5 passes and the DM6Z solid milling tool a total of 12. The force trends are similar to those found for the 4-flute tools, with down-milling operations once showing lower cutting forces. Cutting load values show smaller magnitude for the tool geometry with 6 teeth. More teeth engage the material at any given time, so each tooth experiences less force.

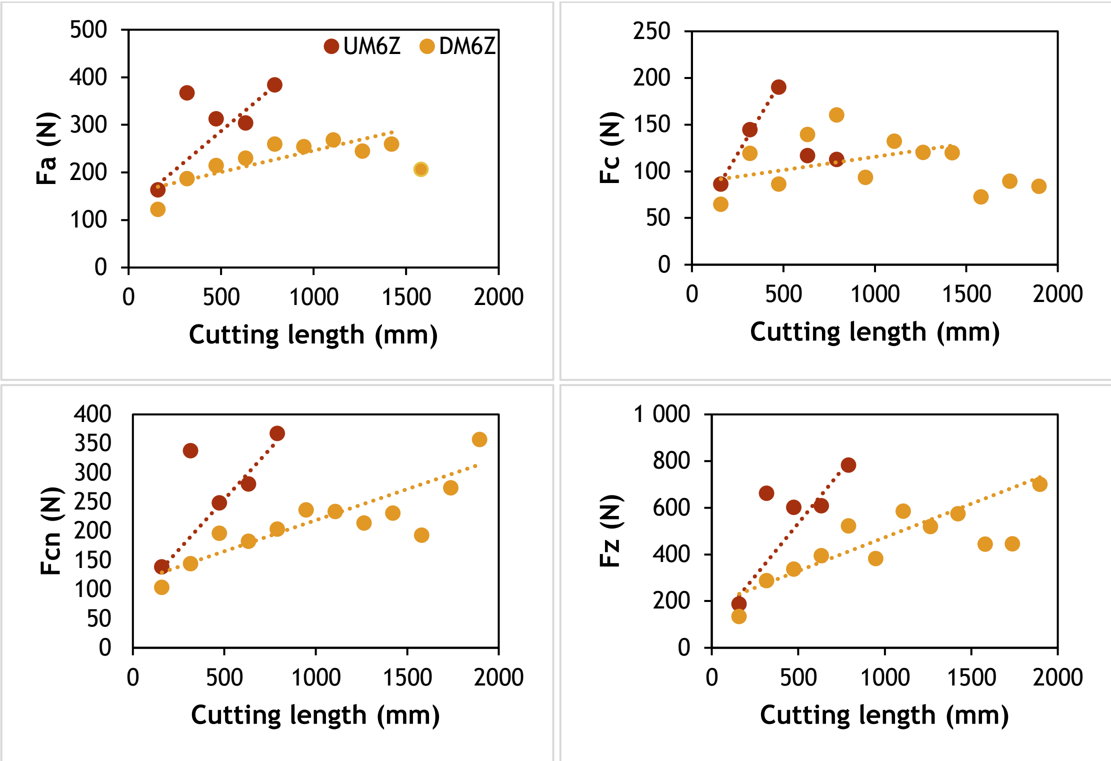

Figure 5.3:Graphical representation of the cutting forces for the UM6Z and DM6Z solid milling tools: F_a (top), F_c (middle left), F_{cn} (middle right) and F_z (bottom)

Figure 5.4 shows, for a cutting length of 1896 mm the difference in cutting loads between spiral and linear milling trajectories. Regardless of the cutting force component being studied, it can be concluded that the spiral path strategy consistently shows lower values when compared to the values collected for the linear strategy. It is possible to infer that reducing the number of tool entries and exits might contribute to this effect (due to wear), which for increasing cutting length promotes very significant differences in the cutting forces.

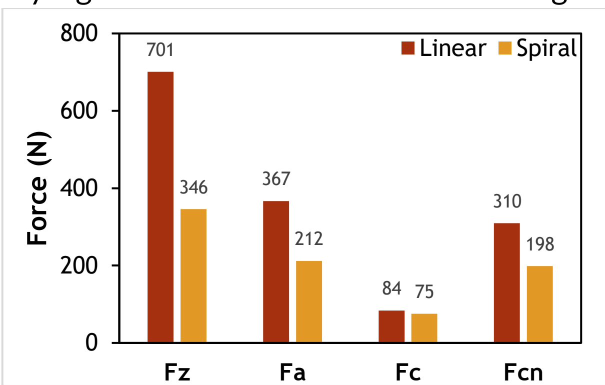

Figure 5.4: Comparison of cutting forces between linear and spiral strategy for a cutting length of 1896 mm, using solid milling tools with the same geometry (6Z) and same cutting parameters (a_p=0.5mm and a_e=1.6mm).

By varying the cutting parameters, there are considerable changes in the measured cutting forces. The different cutting forces recorded for the solid milling tools are shown in Figure 5.5, with the tools identified by the cutting parameters under which they operated.

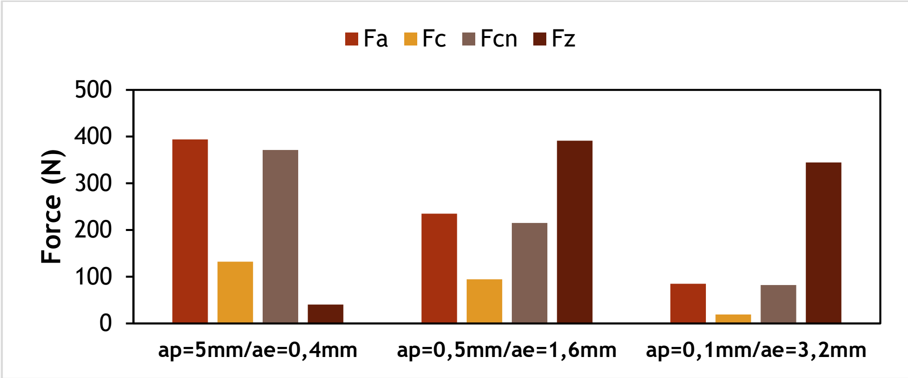

Figure 5.5: Comparison between the different cutting forces for different cutting parameters with the same cutting length (615mm)

The axial depth of cut (a_p) plays a very significant role in the magnitude of the cutting force (F_c), normal to the cutting force (F_{cn}) and, their resultant F_a. A smaller a_p means that less material is being removed during each pass, which results in lower cutting resistance. Since cutting forces are proportional to the chip material volume being removed, reducing the chip volume by decreasing the a_p leads to a smaller magnitude of cutting forces. These results highlight the validity of the experimental cutting tests, given the expected linear evolution of forces according to geometrical definition of uncut chip thickness. Also interesting to note is combined influence of ap and ae in the F_z load. The minimum condition of ae promotes the smallest F_z. Still, na appropriate balance between a_e and a_p seems to be necessary to avoid excessive F_z, which compromises tool life.

These results for the cutting forces of the plane were also verified in the studies by Zimmermann et al. [6], in which the authors justify this trend by the fact that there is an increase in the contact area between the tool and the workpiece.

5.2 Tool wear

During the milling of superalloys, intense mechanical and thermal stresses accelerate tool wear, making this a critical factor that affects tool life. In Table 9, it is possible to find images of the different solid milling tools for the cutting length of 720 mm. The tools that performed down-milling operations show less accumulated wear compared to those that performed up-milling operations, regardless of their geometry.

Alongside the images recorded by digital microscopy, there are polar diagrams of torques recorded for the same cutting length, where the maximum values are found at the cutting edges of the tools. In the DM4Z tool it is possible to clearly identify the location of the cutting edges just by looking at its torque diagram. Meanwhile, in the torque diagram of the DM6Z solid milling tool, a shape very similar to a circle can be observed. This difference (as opposed to the DM4Z) is due to the larger number of teeth and the also larger nose radius of the milling tools, promoting a more distributed load. As was observed in the analysis of the cutting forces, these diagrams also allow us to conclude that the down-milling cutting process is more balanced, this is, having a better cutting torque distribution for all tool edges.

As the solid milling tool accumulates wear, the shape of the diagrams also changes, showing higher values and an evident graphical imbalance, as can be seen in the cutting torque diagrams of the UM4Z and UM6Z tools.

Table 9: Polar diagrams of torque and wear images of the solid milling tools for the cutting length of 790 mm: at the top, UM4Z and UM6Z; at the bottom, DM4Z and DM6Z.

	4Z	6Z
UM	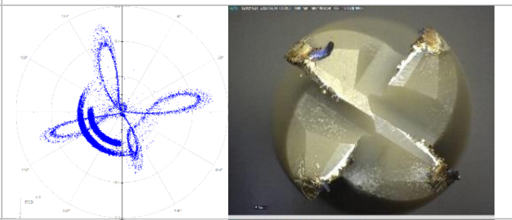	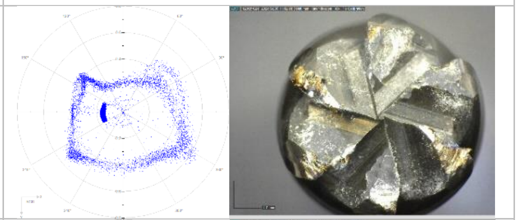
DM	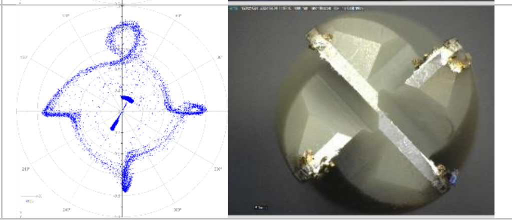	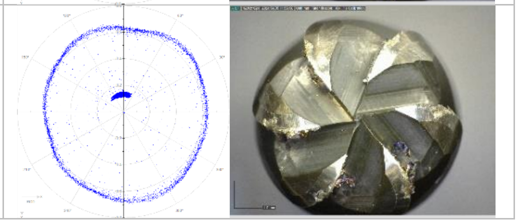

To quantitatively assess the wear suffered by the cutting tools in the various tests the VB criterion was used. For each operation, the wear on each of the teeth was measured and the highest value was used to categorize the wear for that cutting length, with the respective cutting parameters and path strategy.

For the linear path milling strategy, for both geometries, wear always occurred essentially near the top of the solid milling tool, which is why the recorded tool wear images are from this region, as they enable for a better assessment. In the spiral milling strategy, for lower a_p values, wear also occurred preferentially on the cutting edges near the top of the solid milling tool. However, in the experimental test in which an a_p value of 5mm was used, wear was more pronounced on the tool's side, over the length of the a_p value.

As mentioned in Section 4, VB was measured using ImageJ software. As shown in Figure 5.6 (left)**Erro! A origem da referência não foi encontrada.**, two parallel line segments were drawn for each of the tool teeth, comprising all the visible wear between these two segments, with the distance between the lines corresponding to the nominal value of VB. In the situation where greater lateral wear was recorded, as shown in Figure 5.6(right), the measurement was made analogously on the side edges of the solid milling tool.

(a) (b)

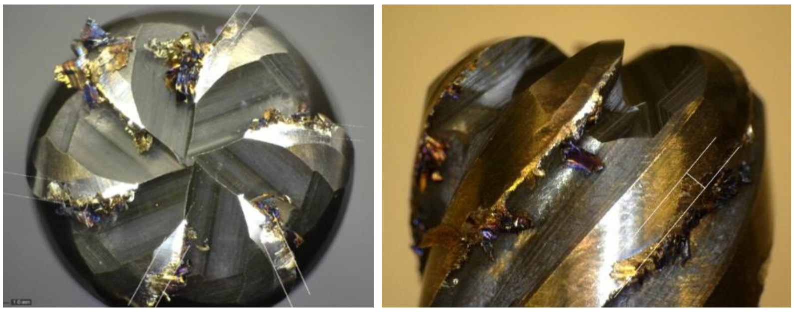

Figure 5.6: Calculation of maximum VB: (a) calculation of the VB on the solid milling tools where there was greater wear on the cutting edges at the top of the tool; (b) calculation of the VB on the solid milling tool that showed greater wear on the side cutting edges.

Figure 5.7 shows the data collected for the solid milling tools used in linear milling. The values show a clear tendency for less wear to occur on tools used for down-milling, regardless of their geometry, as seen in the polar diagrams of cutting torque. The trends for DM4Z and DM6Z are very close, although the DM6Z cutter shows a slightly more stable trend in wear evolution.

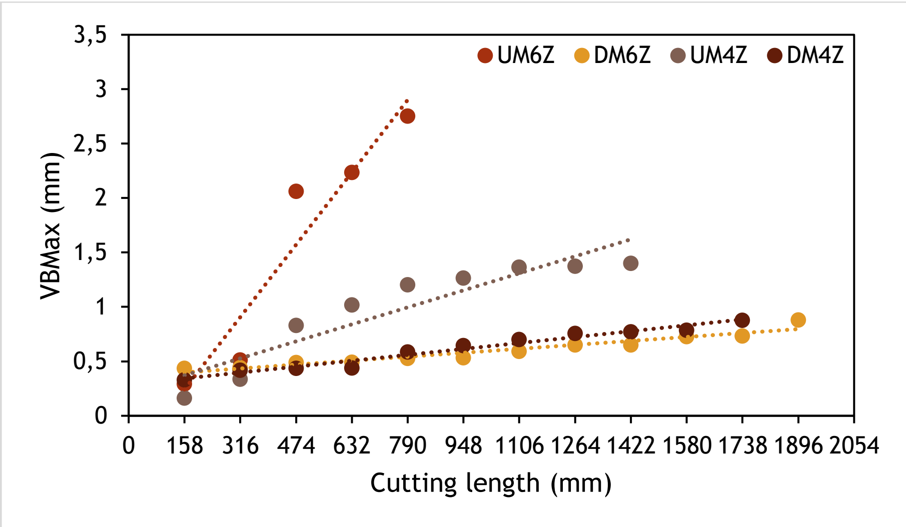

Figure 5.7: VB evolution in a linear trajectory strategy for up-milling and down-milling modes for solid milling tools with 4 and 6 cutting edges.

Since solid milling tools with 6 cutting edges are manufactured with a substrate with a higher percentage of α-phase SiAlON, which gives it greater hardness and therefore greater resistance to wear, may explain the lower wear sustained by the DM6Z tools. These results show that a higher VB is usually associated with higher cutting forces. This was also a conclusion drawn by Huang et al. [34], whose work presents the same evidence.

However, the results obtained for the up-milling operations contradict this hypothesis, but, at the same time, the UM6Z solid milling tool suffered the fracture of one of its teeth at a cutting length of 474 mm, which is believed to have influenced the VB values recorded from that point onwards, making it difficult to understand with any certainty what the actual wear progression would be for this case.

In up-milling operations, there is greater friction between the cutting edge and the workpiece's surface, resulting in an increase in forces and temperature, which promotes the softening of Inconel 718 but also its adhesion to the solid milling tool. This material adhesion occurs irregularly along the cutting edges. Since the cutting process is not continuous but consists of several cycles of thermal and mechanical stresses, when the adhered chips cool down, they become harder and, when they are torn from the tool, they end up also tearing away parts of the substrate (adhesive wear mechanism).

It is worth mentioning that some of the values shown for the solid milling tools with 4 cutting edges in Figure 5.7 are estimated by interpolating their contiguous values, since, sometimes, the measurable VB value did not correspond to the actual value, due to chip adhesion that concealed the sustained flank wear, as also occurred in the studies by Zimmermann et al. [15].

Figure 5.8 shows the graphs with all the measured values and the ones that were interpolated: (a) the values for the up-milling operation are presented; (b) the values for down-milling.

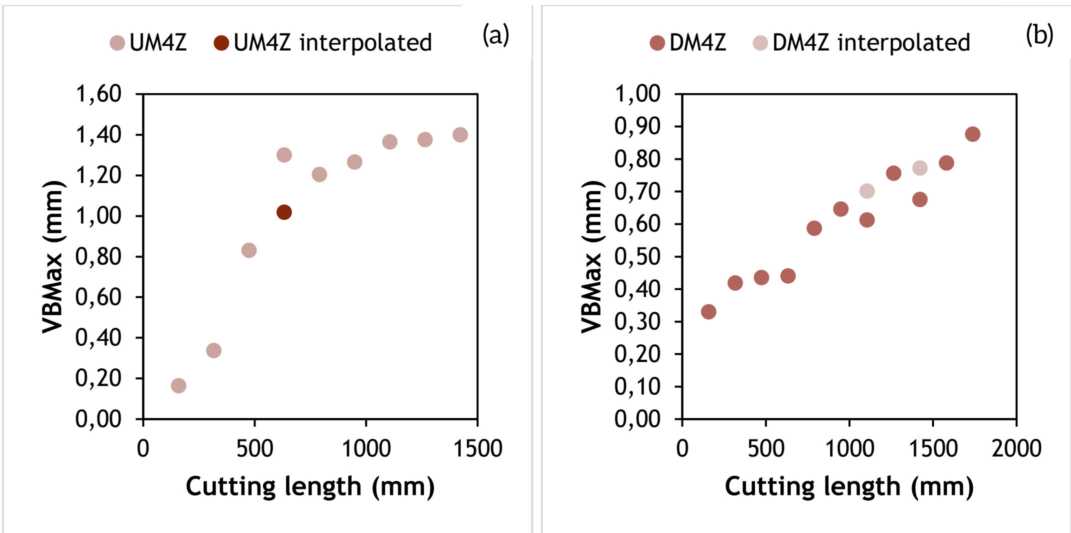

Figure 5.8: Estimated vs Real value of wear for up-milling (a) and down-milling (b) operations with a solid milling tool with 4-teeth.

Since it was impossible to use the measured values to analyze the actual wear progression of the studied tools, it was decided to use an average value, calculated on the basis of the value immediately before and immediately after, this method was applied whenever required.

In order to compare the impact that the milling strategy has on wear, the graph in Figure 5.9 shows the values recorded for a cutting length of 1896 mm, for both studied strategies. It can be seen that by reducing the number of shocks at the entrance to the workpiece (from 12 to just 1), the maximum VB can be reduced to just two thirds of the initial value (while machining more material).

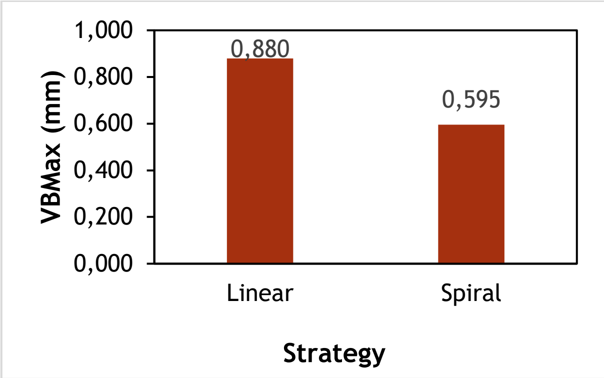

Figure 5.9: Maximum measured VB value in linear vs spiral strategy.

The results obtained are once again in line with those obtained by Huang et al. [34], a higher value of VB is associated with a higher value of cutting forces, since, as seen above, all the cutting forces in the linear strategy were higher than in the spiral strategy.

The polar diagrams of cutting torques for operations conducted with varying cutting parameters are shown in Table 10, accompanied by images of the top-view of the analyzed tools. Contrary to previous observations, these diagrams show the presence of multiple cutting moments. Initially, all diagrams start with lower cutting torque values and a more regular shape, in the center of the diagrams, which changes as the operation progresses and greater wear accumulates, leading to higher cutting torques.

Since the solid milling tool that machined a total length of 5445 mm is the one that shows the most wear, its torque diagram is also more unbalanced at the end of the cutting operation compared to the initial more balanced circular shape.

Table 10: Polar diagrams of torques and wear in spiral milling with different cutting parameters.

615mm	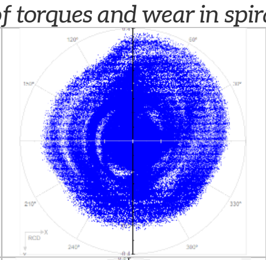	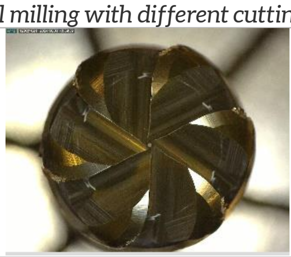
1896mm	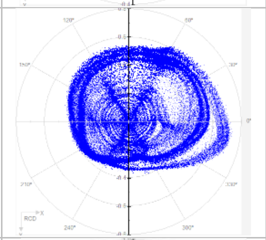	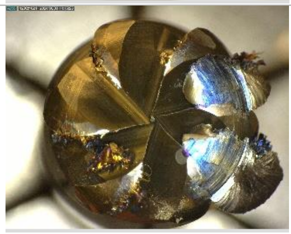
5445mm	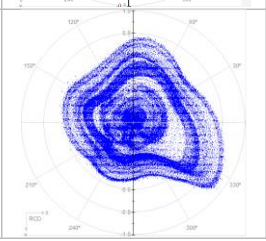	

Figure 5.10 shows the graph with the maximum measured VB values recorded in the tests carried out with these solid milling tools. It is possible to see that the solid milling tool used with a_p of 5 mm is the one with the lowest VB value, but it is also the one that carried out the cutting operation with the shortest length. Again, the solid milling tool that was used with ap of 0.5 mm registered a VB value lower than the one that was used with ap of 0.1 mm, but for a considerably lower cutting length. In fact, according to Hadi et al. [38], higher values of ap imply higher values of VB, although the experimental data collected in this work does not verify this, however, additional cutting tests need to be performed to properly characterize and analyze this.

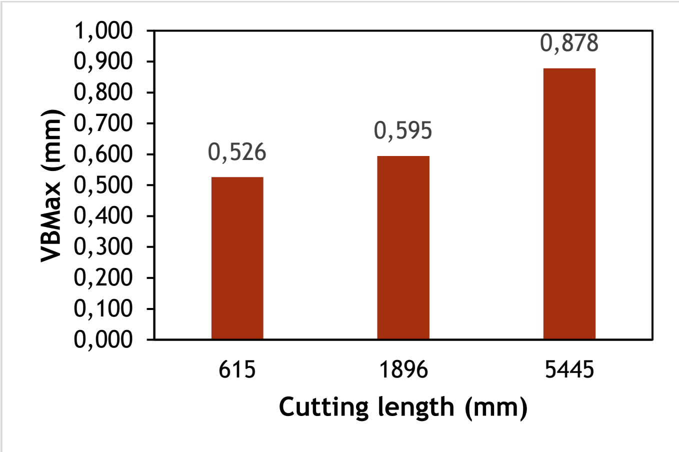

Figure 5.10: VB for solid milling tools that operated with different cutting parameters

5.2.1 Wear Mechanisms

In order to study the wear mechanisms sustained by the different cutting tools during the operations they performed, the solid milling tools were examined, after machining, by scanning electronic microscopy, SEM, equipped with an energy dispersive spectrometer, EDS.

Figure 5.11 shows the flank of one of the UM4Z solid milling tool's teeth Figure 5.11￼A shows that a considerable amount of Inconel 718 has adhered to the tool's surface. In fact, it is thought that a chipping process may have occurred first, leading to the appearance of a crater where the tool material was removed, the appearance of these craters promotes the adhesion of material in the same areas.

By capturing larger images of this region, it is possible to see, in the last picture of Figure 5.11, lighter areas, which correspond to the adhered Inconel 718,Figure 5.11￼-Z1, shows that it is a layer of oxides that has formed on the tool during the milling process, this was concluded thusly by verifying the presence of Oxygen in the obtained EDS spectra.

The existence of these layers of aluminum oxide and titanium oxide is characteristic not only of solid milling tools with 4 edges, but of all the analyzed solid milling tools,Figure 5.12￼ shows the images taken of the UM6Z solid milling tool, where it is also possible to see the existence of three regions, marked Z1, Z2 and Z3.

The EDS analysis of the composition of these three regions is shown in Figure 5.13 . Itcan be seen that Z1 region, made up of Si, Al, O and N, is related to the ceramic tool. In contrast, the most superficial region, Z2, contains chemical elements characteristic of Inconel 718 (chemical composition displayed in Table 1).

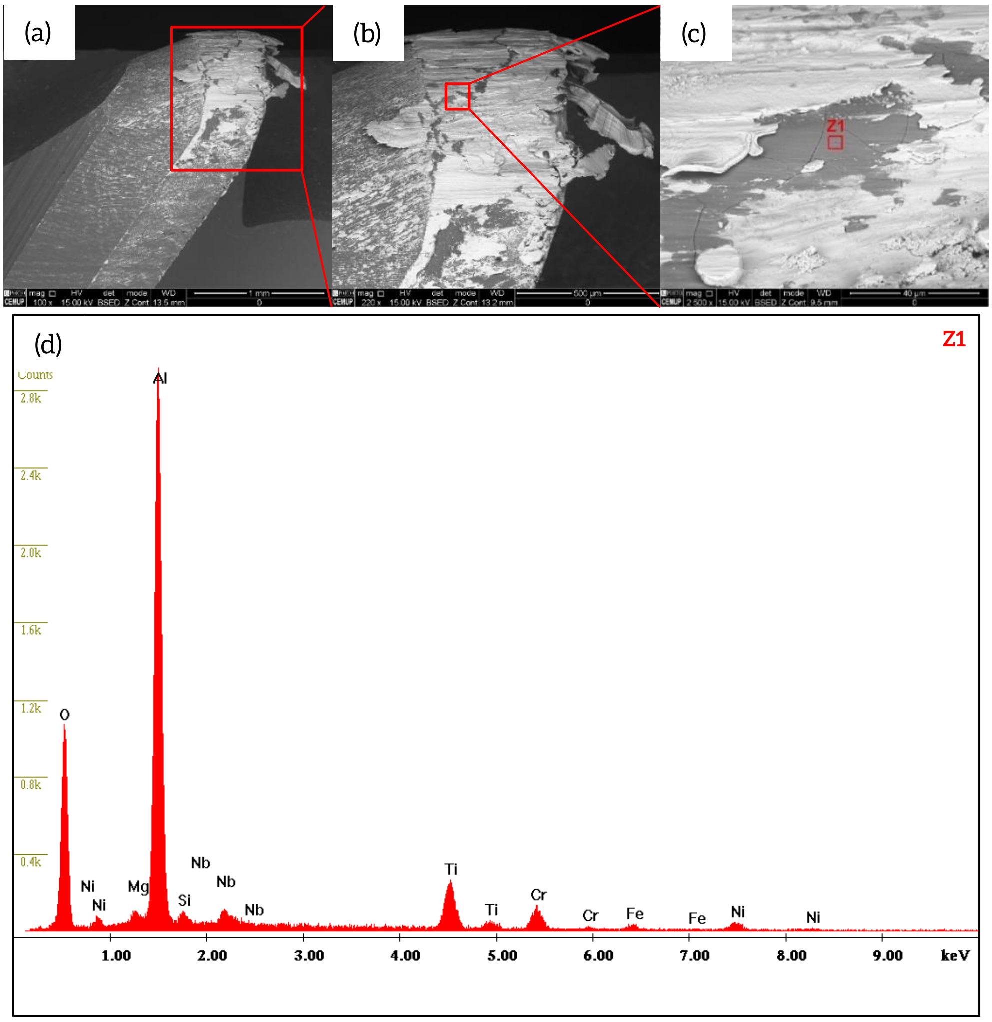

Figure 5.11: Adhesion wear of the UM4Z solid milling tool: (a) flank face of a tool tooth with a amgnification of x100 and (b) with a magnification of x220; (c) oxide layer formed on the surface of the solid milling tool and (d) EDS diagram showing the chemical composition of the oxide layer formed.

The Z3 region mainly displayed the presence of the chemical elements O, Al and Ti, with much higher values than the other elements identified in the analysis. The other present elements are not only from the composition of Inconel 718, such as Nb, Ni and Mo, but also from the cutting tool substrate, such as Si.

Some authors, such as Çelik et al. [26], Huang et al. [34] and Dang et al. [33], point to the existence of a diffusion wear mechanism in Inconel 718 machining processes using ceramic cutting tools at high cutting speeds. The presence of Si in the Z3 region, as shown by the EDS data, may point to the possible appearance of diffusion mechanisms in the tool in the oxide layer between the substrate and the adhered material, which are also partly responsible for the tool's wear.

The appearance of oxide layers was also identified in a study by other authors, [7, 26, 41], and is apparently due to an oxidation process of the solid milling tool when exposed to such high temperatures as those that occur in processes that use this type of tool.

The images in Figure 5.11 and Figure 5.12 show that these oxide layers are fragile, presenting several cracks. These cracks can be attributed to the fact that there are differences in the thermal expansion coefficients of the oxides formed and the SiAlON substrate, as pointed out by Dang et al. [33]. As the milling process with these materials involves high temperatures, the formation of oxidized layers on top of the ceramic substrate takes place and subsequently these layers undergo an abrupt cooling process. Since oxides have higher coefficients of thermal expansion than SiAlON, a sharp drop in temperature will result in a greater reduction in volume, leading to the appearance of cracks.

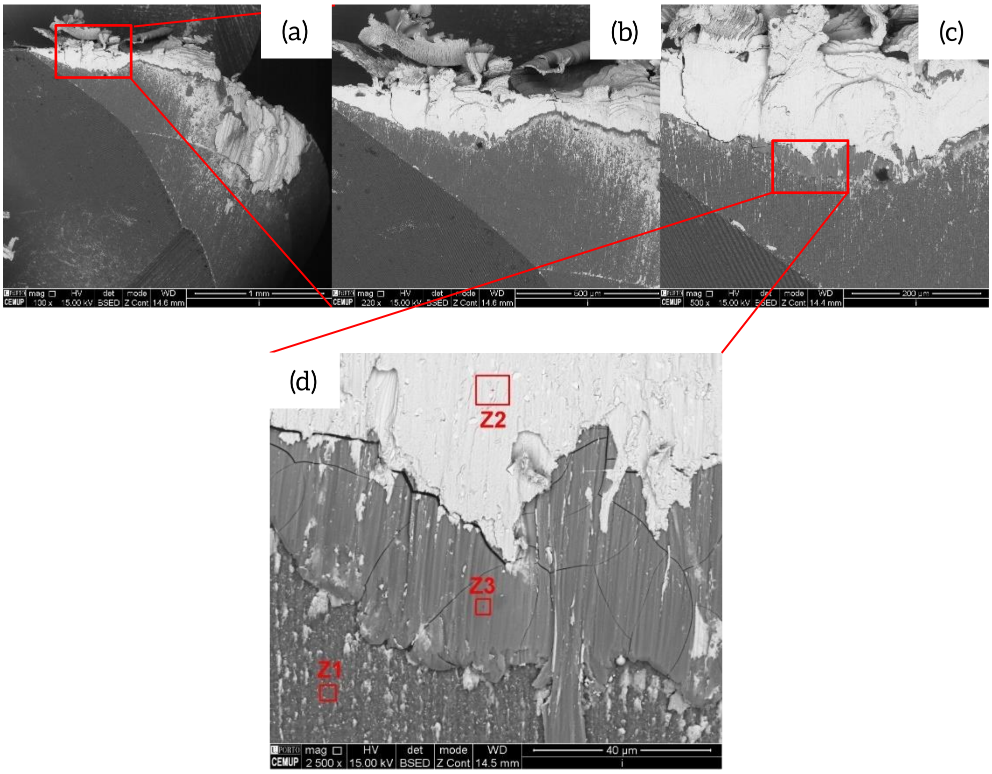

Figure 5.12: Chipping and material adhesion registered on the UM6Z end mill: (a) magnification x100, (b) magnification x220, (c) magnification x500; (d) detail showing the existence of three distinct layers of materials on the surface of the tool (magnification x2500).

Even before analyzing the temperatures involved in the process, the SEM images show that they are high, since the Inconel 718 has been liquefied. As can be seen in Figure 5.14, where some of the material on the tool's surface has the morphology of material that has liquified and solidified (some droplet-shapes are present). Additionally, it is possible to find adhered material on the grinding marks left on the tool's substrate.

Wear mechanisms can also be found on the rake face of the different cutting edges, as shown in Figure 5.15, which shows images of the UM6Z solid milling tool. However, this behavior was found on all the solid milling tools. When compared to the flank, the rake face shows less wear, although it is possible to find crater formation and adhesion of Inconel 718 too. It can thus be seen that the adhered Inconel 718 in this case comes from the chips that are removed from the workpiece during the cutting process, with the characteristic wavy shape.

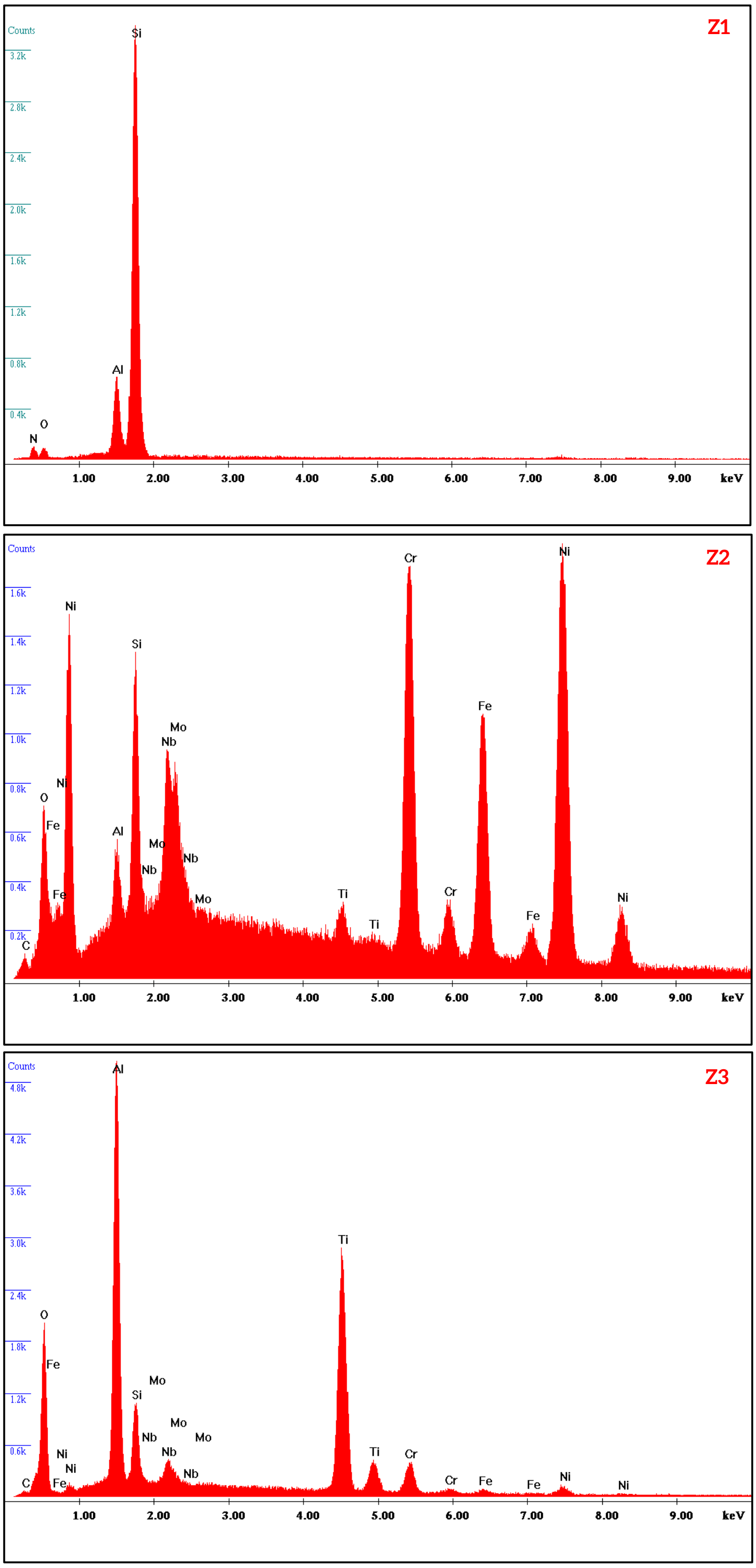

Figure 5.13: EDS of the Z1, Z2 and Z3 regions of the UM6Z end mill

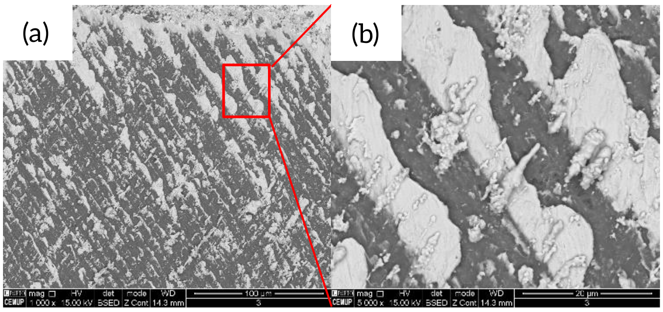

Figure 5.14: Adhesion of material to grinding marks on the DM4Z end mill: (a) flank face of the tool with magnification x1000 and (b) material of Inconel 718 that melted and adhered to the flank face along the grinding lines of the tool (magnification x5000).

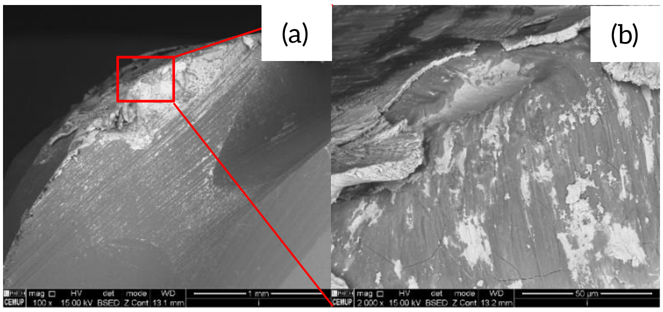

Figure 5.15: Crater formation on the UM6Z end mill: (a) rake face with a crater (magnification x100) and (b) showing some adhered material chips on the cutting edge (magnification x2000).

The images in Figure 5.16 show the presence of several layers of material adhered to the tool, which may reveal that, since milling is an interrupted cutting process, the material adheres in stages, eventually "piling" up. In fact, Çelik et al. [26] identified extensive adhesion phenomena of the material to the solid milling tool, which is then removed during the cutting process, and sometimes resulting in adhesive wear.

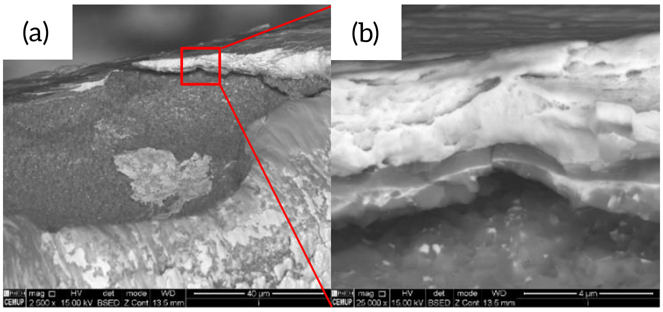

Figure 5.16: Different layers of material adhered to the UM6Z end mill: (a) flank face with layers of material in it (magnification x2500) and (b) .detail of the different existing layers (magnification x25000).

With each pass of the cutting edge through the workpiece, there is material that adheres to the existing material, increasing the thickness of the area. It is believed that it is this adhered material that subsequently detaches from the tool, pulling fragments of it with it, forming craters that will act as a support for the adhesion of new Inconel 718, restarting the cycle.

When comparing the wear of the UM6Z and DM6Z solid milling tools, shown in Figure 5.12 and Figure 5.17, respectively, it is possible to corroborate the information obtained previously by the quantitative study of VB: wear is lower for down-milling operations.

The images in Figure 5.18, which also refer to the DM6Z solid milling tool, clearly show the occurrence of chipping on the cutting edges. According to several authors (as Yishang et al. [36] and Sun et al. [28]), flank wear is the main wear mechanism when milling conducted at cutting speeds above 1000 m/min, but for speeds such as those used in the experimental tests, the mechanisms considered to have the greatest impact are chipping and crater formation.

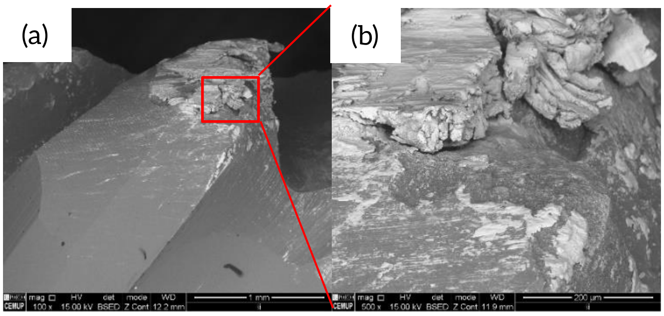

Figure 5.17: Flank wear on the DM6Z end mill: (a) flank face with a magnification x100 and (b) detail of a considerable amount of adhered material (magnification x500).

In fact, except when tooth breakage occurred, it was not the VB assessment that determined whether the tests were finished or not, but the progression of the chipping along the different cutting edges.

Figure 5.18. shows evidence of adhesive wear, where adhered material is detatched during machining taking tool substrate away with it. It is believed that wear is caused, as already mentioned, by material adhering to the tool during different passes of the cutting edge on the workpiece, forming several layers. In these layers, cracks appear and propagate, which then leads to the detachment of the adhered material, thus causing adhesive wear.

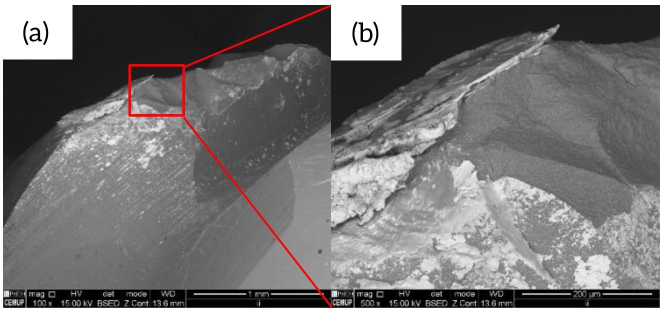

Figure 5.18: Chipping on the DM6Z: (a) image of the rake face (magnification x100) and (b). detail of a cutting edge that underwent chipping (magnification x500).

5.3 Surface Integrity

5.3.1 Roughness

At the end of each machining test, surface roughness of the machined workpiece measurements were performed, the graph in Figure 5.19 shows the average values measured for all linear path strategy tests conducted using the solid milling tools.

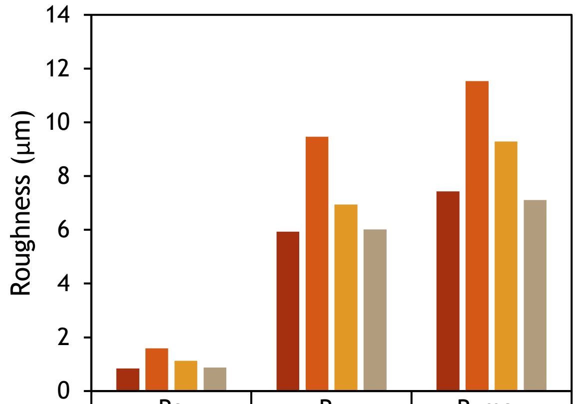

	Ra	Rz	Rzmax
UM4Z (1422mm)	0,8412	5,9278	7,4265
DM4Z (1738mm)	1,5954	9,4698	11,5402
UM6Z (790mm)	1,1225	6,9480	9,2855
DM6Z (1896mm)	0,8768	6,0163	7,1068

Figure 5.19: Roughness for all the solid milling tools used in linear strategy, indicating the respective cutting length.

From the analysis of the values in Figure 5.19, it is possible to conclude that in down-milling operations, the solid milling tool with 6 cutting edges shows lower values for all the studied roughness parameters compared to the 4-teeth tool. In up-milling operations, the trend is the opposite, with the 4-teeth solid milling tool recording better surface quality for up-milling mode. However, it is important to note that the variation in surface roughness value from up-milling to down-milling observed for the 4Z tools is greater than the difference registered for the 6Z tools, despite these having opposing trends.

The surface roughness of the machined workpieces is influenced not only by the cutting forces and the vibration inherent to the milling process but also significantly by the inclusion of removed chips at the cutting operation, which are welded onto the new surface created. This adhered chip will greatly affect the tool life of the solid milling tool and, in turn, further deteriorate the machined surface quality.

Another aspect to consider in this analysis is the existence of burr production, which ultimately has the same effect on surface quality and tool life as the adhered chip. This linear trajectory strategy involved an entry and exit from the workpiece, which would increasingly promote the formation of burr with each pass. The existence of this burr may explain the increasing F_a values as the cutting length increases, as already seen. Figure 5.20 shows the burr that can be found at the end of some operations. For cutting lengths of 790 and 1580 mm, the accumulated burr was so considerable that it was decided, after each linear test was concluded, to make an extra machining pass with a different tool to remove this type of defect.

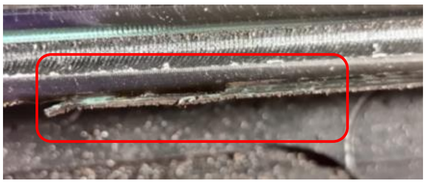

Figure 5.20: Burr found at 790 mm of cut length when machining in a linear strategy.

5.3.2 Microstructure

Regarding microstructure, after the cutting operations using the linear path strategy, two samples were cut from the workpiece so that their microstructure could be analyzed. Figure 5.21 shows the optical microscope images of these two samples. Figure 5.21A and Figure 5.21B show the Inconel 718 undeformed microstructure. Figure 5.21C and D show microstructure cross-section of the machined surface. It can be seen that, when comparing the surface images with those taken from further inside the workpiece, the surface microstructure shows grain refinement and distortion. This distortion favours one direction, this being the direction of the machining tool, as shown in Figure 5.21C.

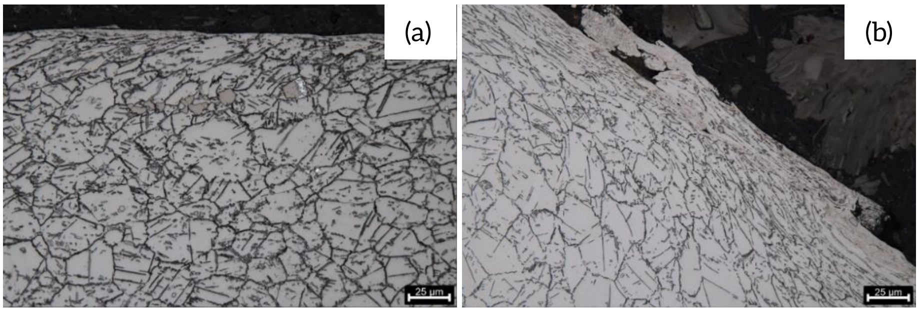

Figure 5.21: Microstructure of the sample 1 (a) and 2 (b) on the machined surface

These results were also found by several authors in their studies, such as Zimmermann et al. [6] and Finkeldei et al. [19]. Both authors found grain deformation near the machined surface and an elongated grain orientation in the feed direction. It is relevant to mention that this grain refinement and deformation is heavily tied to the machining speeds that are used during cutting, with higher machining speeds promoting more grain deformation. Of course, cutting temperature also plays a role in this phenomenon, as it promotes material softening (furthermore, high cutting speeds generate higher cutting temperatures).

5.4 Temperature

The Optris PIX Connect software was used to collect and export the temperature data acquired during testing. In order to estimate differences in the cutting temperature for the solid milling tools used in a linear strategy, the average temperature of the area corresponding to the machined surface (as shown in Figure 5.22) was monitored during one tool passage. Figure 5.23 presents those results.

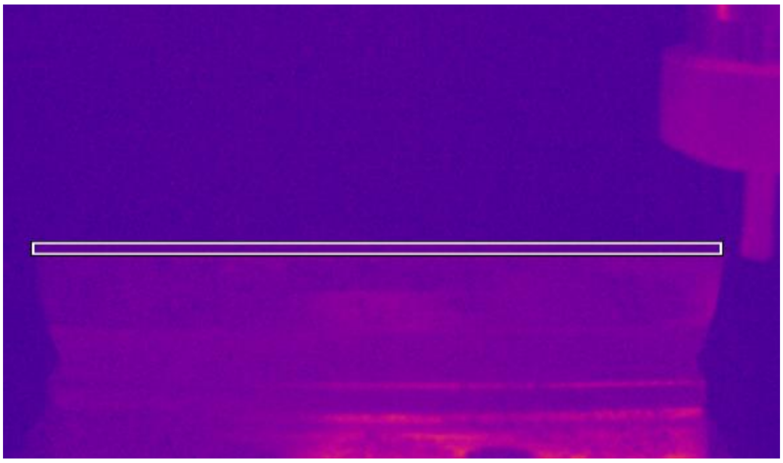

Figure 5.22: Tracked area (machined surface) for average temperature calculation.

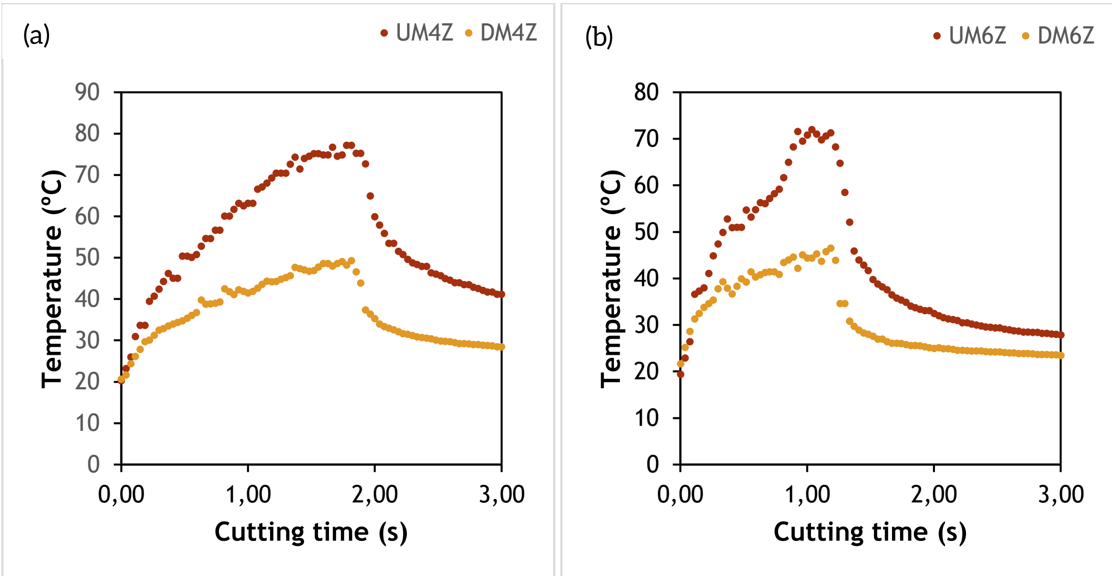

Figure 5.23: Cutting temperatures recorded for the same cutting length for solid milling tools with 4 teeth (a) and with 6 teeth (b).

It is possible to observe that, regardless of the geometry of the solid milling tool, up-milling operations record a higher average temperature than down-milling operations, with a difference of about 25°C. The difference between the average temperatures for tools with 4 cutting edges and those with 6 cutting edges is negligible.

Considering that the high temperatures recorded are due to the high deformation rates of Inconel 718, which has very low thermal conductivity, all the heat generated by the plastic deformation tends not to dissipate easily, leading to an increase in temperatures during the cutting process. These high temperatures in the workpiece contribute to increased temperatures in the cutting tool as well, influencing its wear and lifespan. According to these considerations and the information presented in the graphs, down-milling operations appear to be more advantageous for the solid milling tools.

Since the thermal camera, in the milling operations with a spiral strategy, was mounted on the tool spindle, it was possible to analyze the temperature evolution on the area of the solid milling tool. Figure 5.24 shows this area, and the data collected for the average temperatures in these milling operations are presented in Figure 5.25.

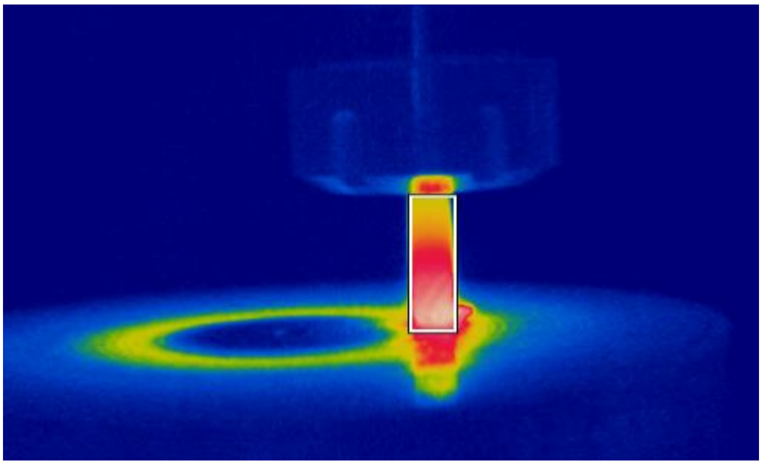

Figure 5.24: Selected area for temperature measurement in milling operations with a spiral strategy

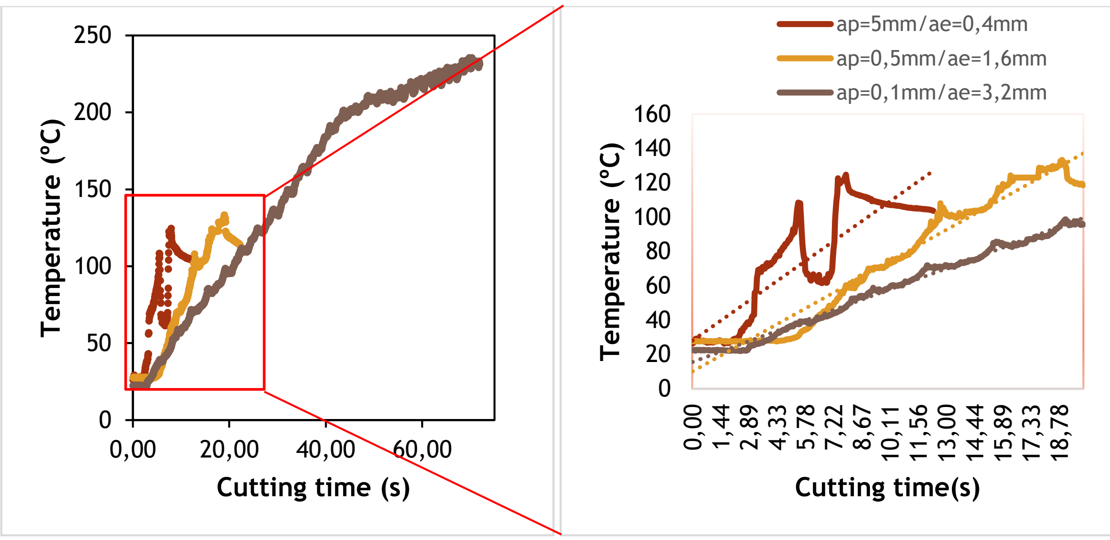

Figure 5.25: Cutting temperatures recorded in milling operations with a spiral strategy for the different tested parameters (a) and trends in the evolution of each solid milling tool with increasing cutting time (b).

When comparing the average temperatures shown in Figure 5.25, it is evident that the solid milling tool with the fastest increase in values was the one that operated with the highest a_p and performed a total cutting length of 615 mm. In fact, the maximum average temperature recorded by this solid milling tool was only reached by the tool operating with an intermediate a_p after double the cutting time. There is thus a trend toward a more controlled evolution of average temperatures with the reduction of a_p (and the increase in a_e).

5.5 MRR and Material Removed

The material removal rate is able to offer an unbiased comparison of the performance of all solid milling tools, since it reflects the volume of material that is removed per unit of time. This performance evaluation criterion is therefore independent of the time the machining is carried out, i.e. independent of the cutting length. Figure 5.26 shows the MRR values for each of the tools used in the tests.

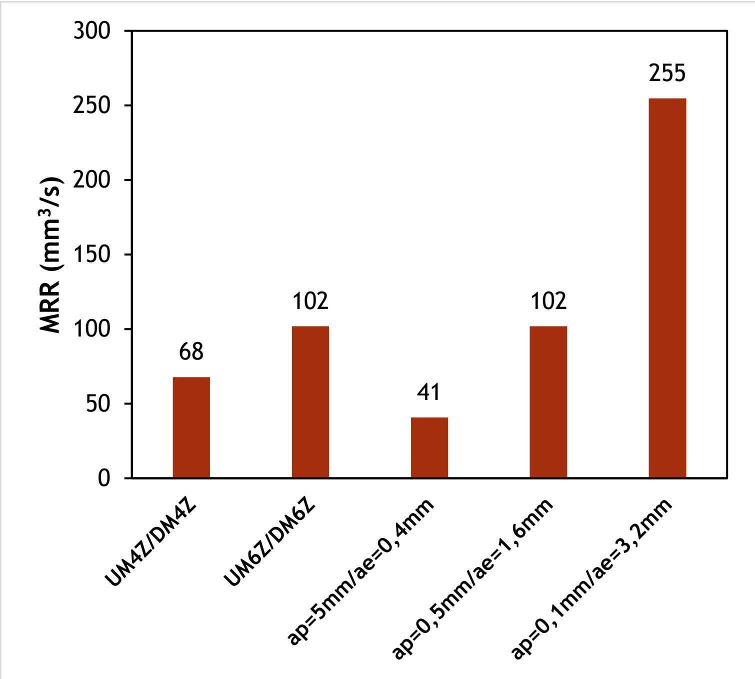

Figure 5.26: Material Removal Rate (MRR) for all the studied solid milling tools.

The 4-edged solid milling tools used the same cutting parameters, with the only difference being that one was down-milling and the other up-milling, so the MRR was the same for both. Similarly, the 6-tooth tools that carried out the cutting operations with a linear path strategy also have the same MRR value, as the parameters were the same. Between the two, it can be seen that the most advantageous situation is that of cutting with 6-tooth tools.

In fact, the MRR value is obtained by dividing the machined volume by the machining time. Solid milling tools with 6-tooth have a higher linear speed than 4-tooth solid milling tools since this parameter depends on the number of teeth, as shown in Equation 5.

For the tools that were used in spiral path strategies, the number of cutting edges remains the same, but here it is the cutting parameters that are changed, which is reflected in a higher or lower rate. Even so, the MRR values for these three cutters follow the trend: solid milling tools with a smaller ap but larger ae allow for a higher MRR.

When all the data in the graph is compared, it can be seen that the lowest MRR value is shown by the solid milling tool that used a_p=5mm and a_e=0.4mm, followed by the 4-tooth solid milling tools. There is no variation between the

UM6Z/DM6Z tools and the solid milling tool that used a_p=0.5mm and a_e=1.6mm, since the cutting parameters are the same (the only thing that changes is the milling strategy).

The one with the highest MRR value, which in theory equates to more efficient performance, is the solid milling tool that used a_p=0.1mm and a_e=3.2mm, which may indicate that these tools with this geometry are more suitable for this type of machining operation: operations with an extreme value of ae or ap, with the other parameter being the lowest possible.

Although MRR is a commonly used measure of efficiency in the industry, it does not account for the wear the tool experiences during cutting, and cannot, on its own, indicate which parameter combination will lead to higher productivity. The volume of material effectively removed is a measure that combines the material removal rate with the wear the tool undergoes under those conditions.

The volume of material actually removed was different in the tests carried out with different solid milling tools in the linear path strategy. The graph in Figure 5.27 shows the different volumes machined for each solid milling tool (in linear strategies). With a_p set at 0.5mm and a_e at 1.6mm, each step, in which a 158mm cutting length was machined, corresponds to a removed volume of 126.40mm^3.

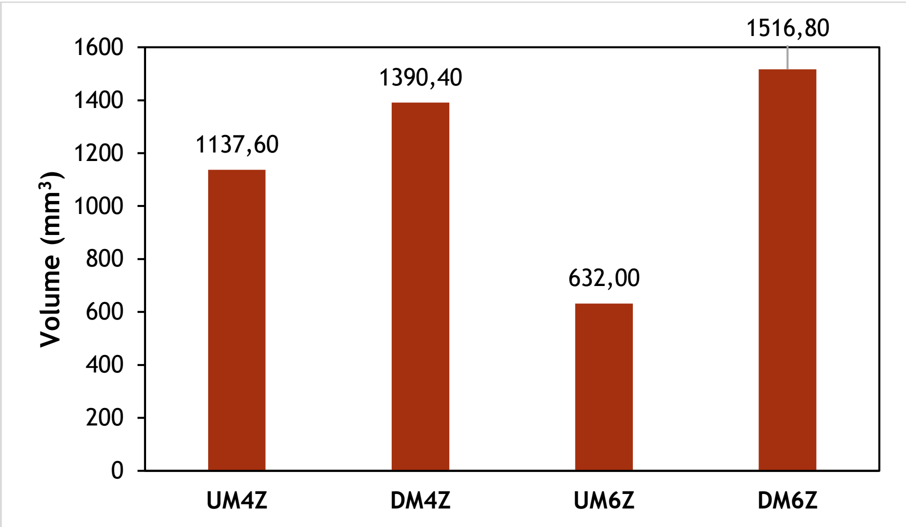

Figure 5.27: Volume of material effectively removed by all the solid milling tools used in linear strategy during the tests conducted

Of all of them, the cutter with the lowest value removed was the UM6Z, since it also performed the lower number of steps, only 5. So, unsurprisingly, the tool with the highest total volume removed was the DM6Z with a value of 1516.80mm^3. In terms of the efficiency of the cutting process, the down-milling mode allows for larger volumes to be removed, regardless of the geometry of the solid milling tools, as it exhibits a more controlled wear progression and, therefore, enables more steps to be performed before failure.

With the change in cutting parameters and the consequent change in the expected lengths of the cutting operations, the actual volumes that were removed from the workpiece in spiral strategy are no longer a variable that reflects the efficiency of each of the processes. Therefore, in order to analyze this measure, only one time interval common to all three tests was considered: 5 seconds. From the values shown in Figure 5.28, the tool that removed the least material was solid milling tool which carried out shouldering operations, using a_p=5mm and a_e=0.4mm, and it was the tool whose parameters would be part box opening parameters (a_p=0.1mm and a_e=3.2mm) that was able to remove the maximum amount of material in the time interval considered.

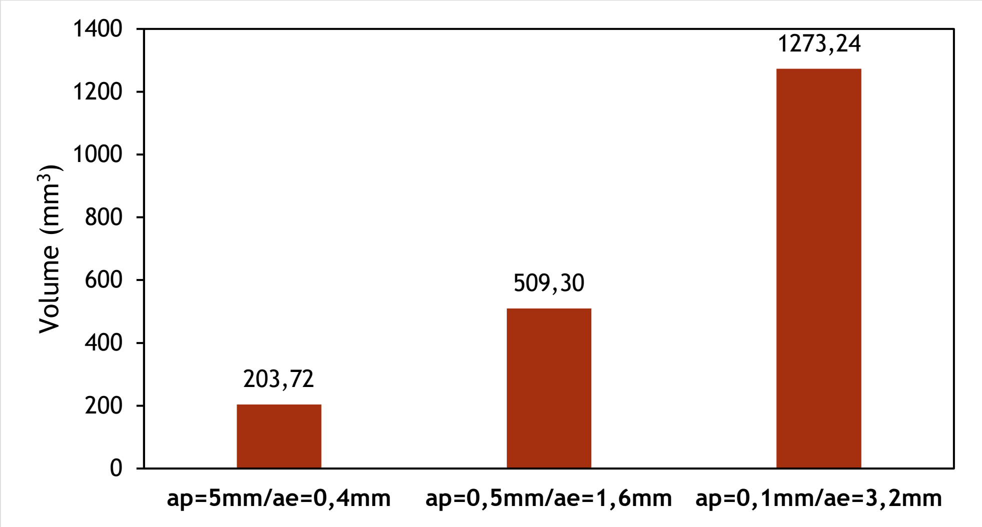

Figure 5.28: Volume of material effectively removed after 5 seconds for each of the tested combinations of a_p and a_e.

In fact, some authors have concluded in their studies [15, 19] that cutting tools made of SiAlON are more efficient, when compared to the use of solid carbide milling tools, because they allow machining at much higher cutting speeds than conventional tools and accepted higher cutting parameters.

5.6 Tool-workpiece interface pressure and temperature

In order to understand pressure and temperature evolutions at the tool-workpiece interface, the tool has been discretized in 20 points along its edge, as shown in Figure 5.29.

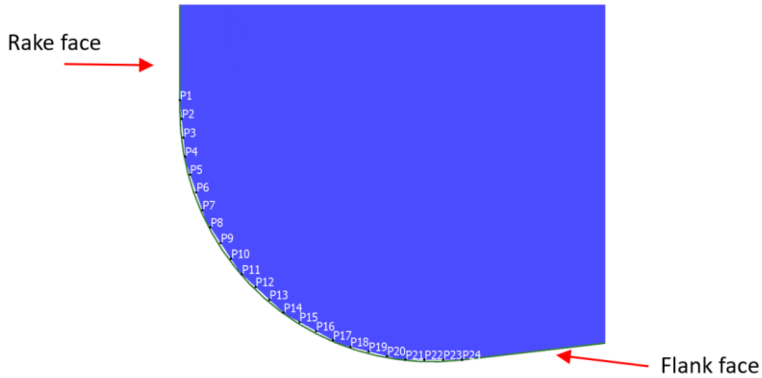

Figure 5.29. Cutting edge region discretization for tool-interface pressure and temperature numerical estimation.

Figure 5.30 presents the results of contact pressures and temperatures at the interface between the cutting tool and the workpiece, depending on the milling mode, as obtained through the numerical model (average of the tracked points in Figure 5.29). The evolution of these variables over the trajectory of one single cutting edge helps to understand the differences in tool life between down-milling and up-milling. The main difference between these two milling modes lies in the temporal sequence between the moments when the interface pressure and temperature reach their maximum on the cutting tool edge during the cutting process. In down-milling, the moment of maximum pressure in the cutting zone differs from the moment of maximum tool temperature. As such, when the contact pressure is at its peak, the temperature remains relatively low, despite a sharp rising trend. In up-milling, the maximum contact pressure is applied to the tool when the temperature is also approaching its peak, thereby contributing to the rapid deterioration of the cutting edge. The temporal sequence of thermomechanical effects corroborates the more severe operating conditions faced by tools subjected to up-milling.

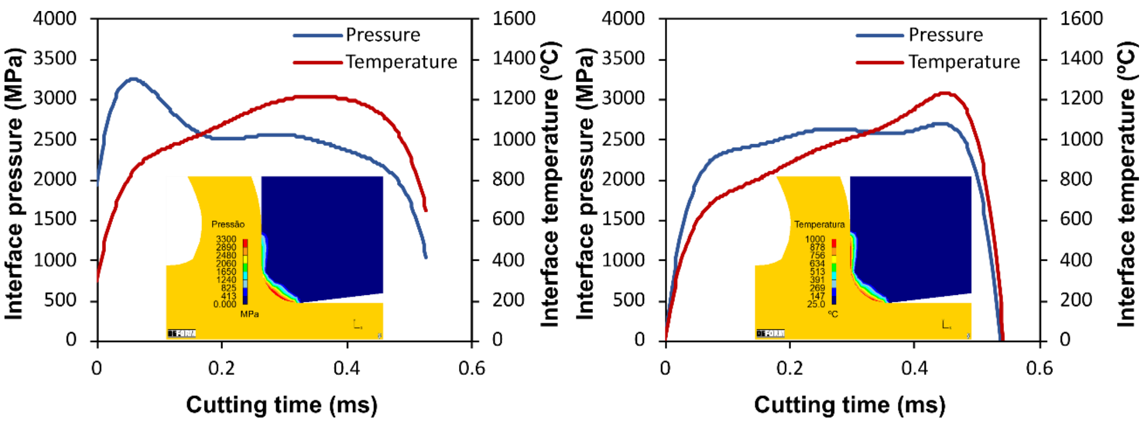

Figure 5.30. Contact pressures and temperatures at interface between the cutting tool and the workpiece, depending on the milling mode: down-milling (a) and up-milling (b).

Simulation results regarding contact pressure on the tool surface show a maximum value for the down-milling process, whereas up-milling results in the highest interface temperature. The temperature increase observed at the end of the up-milling process can be considered a real effect and not merely a numerical singularity, as the same phenomenon is visible in the experimental results obtained via thermographic imaging (refer to Figure 5.23) which displays the average temperature increase on the machined surface after one pass of the cutter. Although this is not a direct measure of the tool temperature, the comparison of average temperatures allows for distinguishing between up-milling and down-milling in terms of average temperatures observed in an area circumscribed to the machined track. It is noticeable that this average temperature is approximately 20°C higher in the case of up-milling. The temperature increase can be explained by the high strain rates of the chip during cutting. The high strain rates imposed on the workpiece material lead to an increased mechanical response and, consequently, greater heat generation due to plastic deformation. Indirectly, up-milling appears to generate a higher level of plastic deformation, which in turn promotes rapid tool degradation due to the close temporal proximity of maximum thermal and mechanical loads.

6 Conclusions

This chapter presents the conclusions drawn from the study of milling Inconel 718 using solid end mills made of SiAlON. Based on the experimental results and numerical simulations conducted, it is possible to evaluate the performance of these ceramic tools, which are considered a promising alternative to traditional cutting materials due to their wear resistance and ability to operate under severe cutting conditions. The main observations regarding the behavior of the tools in different milling strategies and modes, as well as the influence of cutting parameters on tool wear and machined surface quality, are listed in this chapter, providing a comprehensive overview of the benefits and limitations of using SiAlON in the machining of nickel-based superalloys.

Based on the results obtained from the experimental tests, solid milling tools made exclusively from SiAlON have proven to deliver promising results in terms of productivity and efficiency. In fact, by maintaining their mechanical properties even at high temperatures, they are able to perform milling operations at high cutting speeds, even on materials with low thermal conductivity, such as Inconel 718.

When comparing the two milling modes studied, the results recorded for down-milling, whether in terms of cutting forces, temperatures, or wear, are consistently lower and show a more controlled trend of evolution.

The spiral milling strategy proves to be more advantageous when compared to the linear trajectory strategy, as it eliminates the impact of the tool's entry into the workpiece, allowing for a longer uninterrupted cutting length. Given that the material is less resistant to impact, the difference between the two strategies is evident in a direct comparison, with the spiral strategy resulting in less wear and a longer tool life.

Among the three combinations of a_p and a_e tested, the solid milling tools that operated with high values for either parameter demonstrated better performance. However, among the tests carried out, the operation where $a_p \ll a_e$ resulted in less tool wear, allowing for longer operation time and achieving a greater material removal volume from the workpiece. In contrast, the combination of $a_p \gg a_e$ showed a much faster temperature rise and greater wear.

Due to the low thermal conductivity of Inconel 718, the cutting process—which inherently generates significant plastic deformation—results in extremely high temperatures. These elevated temperatures not only facilitate the softening of the nickel superalloy but can also lead to a phase change, resulting in widespread adhesion phenomena on the various solid milling tools. This adhesion significantly contributes to tool failure. In addition to adhesion wear, which proved to be the predominant wear mechanism, evidence of abrasion wear, as well as chipping of the cutting edges and crater formation on both the rake face and the flank face, was also observed.

Although SiAlON tools offer a highly attractive productivity rate for the industry, their performance is often compromised by the projection of chips formed at high speeds and their subsequent embedding into the already-machined surface. This frequently results in workpieces with suboptimal surface quality.

The simplification of the milling process to a 2D orthogonal cutting model proved effective in predicting cutting forces when compared to experimental values. This approach enabled the analysis of temperature behavior and cutting pressure throughout the passage of a single tooth across the workpiece. It provided insights into the reasons behind the differences observed, such as in wear and cutting temperatures, across different milling modes, helping to understand down-milling is ultimately more advantageous, given the

7 Future work

Despite this study providing a clearer view of some key aspects of milling superalloys, particularly Inconel 718, there are still several paths that can be explored in the future. The following is a summary list of some of them.

- **Coated tools:** One of the most relevant aspects and one of the most frequently mentioned scenarios by most authors in the study of Inconel 718 is the occurrence of adhesion on tools. The study of ceramic tools with coatings and the comparison of the data obtained with those made solely from SiAlON could provide essential new insights into this topic. Coatings can be an excellent contribution to reducing wear and increasing the toughness of cutting tools.
- **Milling Strategies**: In addition to studying cutting operations performed with linear or spiral strategies, other options such as trochoidal strategy may yield more promising results in making the milling process more efficient in an industrial context.
- **Vibration Analysis**: The axial component was mentioned in this study; however, it was not explored in depth, nor were detailed explanations provided for the reasons why its values were higher than those of the cutting force. The presence of vibrations during the cutting process, which are theoretically expected to increase with higher cutting speeds, is a critical factor. Further research in this area could provide valuable new insights.
- **Parameter Optimization**: In addition to the parameter combinations used in this study, there are various other combinations that could yield equally or more promising results. Furthermore, given the limited number of solid milling tools available and the timeframe of the study, a deeper analysis of the results indicated by the experimental tests seems essential. Repeating the experiments with a common cutting time for several tools could make the wear and tool life data more comparable and beneficial.
- **Environmental Impact**: One of the reasons for using ceramic solid milling tools is their advantage of not requiring cutting fluids for operations at high speeds. However, the environmental impact of cutting tools extends beyond the use of cutting fluids. Studying the entire lifecycle of these tools, from the procurement of raw materials to their end-of-life disposal, could be important for understanding and potentially reducing their environmental impact.

References

1. Liu, C., et al., *Chip formation mechanism of Inconel 718: a review of models and approaches.* Chinese Journal of Mechanical Engineering, 2021. **34**: p. 1-16.
2. Rahman, M., W. Seah, and T. Teo, *The machinability of Inconel 718.* Journal of materials processing technology, 1997. **63**(1-3): p. 199-204.
3. De Bartolomeis, A., et al., *Future research directions in the machining of Inconel 718.* Journal of Materials Processing Technology, 2021. **297**: p. 117260.
4. Thakur, D., B. Ramamoorthy, and L. Vijayaraghavan, *Machinability investigation of Inconel 718 in high-speed turning.* The International Journal of Advanced Manufacturing Technology, 2009. **45**: p. 421-429.
5. Davim, J.P., *Machining of hard materials*. 2011: Springer Science & Business Media.
6. Zimmermann, R., et al., *Surface integrity in high-feed roughing of Inconel 718 with SiAlON end mills.* Procedia CIRP, 2022. **108**: p. 595-600.
7. Roy, S., et al., *A brief review on machining of Inconel 718.* Materials today: proceedings, 2018. **5**(9): p. 18664-18673.
8. Kar, B.C., et al., *Research trends in high speed milling of metal alloys: A short review.* Materials Today: Proceedings, 2020. **26**: p. 2657-2662.
9. Chauhan, S., R. Trehan, and R.P. Singh, *State of the art in finite element approaches for milling process: a review.* Advances in Manufacturing, 2023. **11**(4): p. 708-751.
10. Sandvik. *Fresamento concordante vs. fresamento discordante*. 18-05-2024]; Available from: https://www.sandvik.coromant.com/pt-pt/knowledge/milling/down-milling-vs-up-milling.
11. Klocke, F., F. Klocke, and A. Kuchle, *Cutting tool materials and tools.* Manufacturing Processes 1: Cutting, 2011: p. 95-196.
12. Wang, B. and Z. Liu, *Influences of tool structure, tool material and tool wear on machined surface integrity during turning and milling of titanium and nickel alloys: a review.* The International Journal of Advanced Manufacturing Technology, 2018. **98**: p. 1925-1975.
13. Ma, Z., et al., *Cutting performance and tool wear of SiAlON and TiC-whisker-reinforced Si3N4 ceramic tools in side milling Inconel 718.* Ceramics International, 2022. **48**(3): p. 3096-3108.
14. Arunachalam, R. and M. Mannan, *Machinability of nickel-based high temperature alloys.* Machining science and technology, 2000. **4**(1): p. 127-168.

15. Zimmermann, R., et al., *Tool wear progression of SiAlON ceramic end mills in five-axis high-feed rough machining of an Inconel 718 BLISK.* Procedia CIRP, 2021. **101**: p. 13-16.
16. Xu, D., et al., *Investigation of the influence of tool rake angles on machining of inconel 718.* Journal of Manufacturing and Materials Processing, 2021. **5**(3): p. 100.
17. Celaya, A., et al. *Influence of cutting edge radius on tool life in milling Inconel 718*. in *AIP Conference Proceedings*. 2019. AIP Publishing.
18. Thakur, A. and S. Gangopadhyay, *State-of-the-art in surface integrity in machining of nickel-based super alloys.* International Journal of Machine Tools and Manufacture, 2016. **100**: p. 25-54.
19. Finkeldei, D., M. Sexauer, and F. Bleicher, *End milling of Inconel 718 using solid Si3N4 ceramic cutting tools.* Procedia CIRP, 2019. **81**: p. 1131-1135.
20. Mandal, H., *New developments in* α*-SiAlON ceramics.* Journal of the European Ceramic Society, 1999. **19**(13-14): p. 2349-2357.
21. Xu, W., et al., *Optimized design of structural parameters of Si3N4-based ceramic tools with variable cross-section.* Ceramics International, 2023. **49**(4): p. 6238-6245.
22. Zhao, B., et al., *Tribological behavior of three silicon nitride ceramics in dry sliding contact against Inconel 718 over a wide range of velocities.* Wear, 2020. **448**: p. 203206.
23. Guo, F., et al., *Cutting performance of a new spark plasma sintered SiAlON ceramic tool for high-speed milling of Inconel 718.* The International Journal of Advanced Manufacturing Technology, 2022. **119**(11): p. 7327-7338.
24. Izhevskiy, V., et al., *Progress in SiAlON ceramics.* Journal of the European Ceramic Society, 2000. **20**(13): p. 2275-2295.
25. Bitterlich, B., S. Bitsch, and K. Friederich, *SiAlON based ceramic cutting tools.* Journal of the European Ceramic Society, 2008. **28**(5): p. 989-994.
26. Çelik, A., et al., *Wear behavior of solid SiAlON milling tools during high speed milling of Inconel 718.* Wear, 2017. **378**: p. 58-67.
27. Sarıkaya, M., et al., *A state-of-the-art review on tool wear and surface integrity characteristics in machining of superalloys.* CIRP Journal of Manufacturing Science and Technology, 2021. **35**: p. 624-658.
28. Sun, H., B. Zou, and W. Chen, *Cutting performance of silicon-based ceramic end milling tools in high-efficiency machining of GH4099 under dry condition.* The International Journal of Advanced Manufacturing Technology, 2022: p. 1-14.
29. Ezugwu, E., Z. Wang, and A. Machado, *The machinability of nickel-based alloys: a review.* Journal of Materials Processing Technology, 1999. **86**(1-3): p. 1-16.

30. Zhao, B., et al., *High temperature tribological properties of silicon nitride in dry sliding contact against Inconel 718 heated by laser.* Wear, 2019. **434**: p. 203000.
31. Zheng, G. and J. Zhao, *Performance of Sialon/Si3N4 graded ceramic tools at high speed machining*, in *High Speed Machining*. 2020, Elsevier. p. 27-62.
32. Molaiekiya, F., et al., *Influence of process parameters on the cutting performance of SiAlON ceramic tools during high-speed dry face milling of hardened Inconel 718.* The International Journal of Advanced Manufacturing Technology, 2019. **105**: p. 1083-1098.
33. Dang, J., et al., *New observations on wear characteristics of solid Al2O3/Si3N4 ceramic tool in high speed milling of additive manufactured Ti6Al4V.* Ceramics International, 2020. **46**(5): p. 5876-5886.
34. Huang, X., et al., *Wear mechanisms and effects of monolithic Sialon ceramic tools in side milling of superalloy FGH96.* Ceramics International, 2020. **46**(17): p. 26813-26822.
35. Parenti, P., et al., *An experimental investigation on Inconel 718 interrupted cutting with ceramic solid end mills.* The International Journal of Advanced Manufacturing Technology, 2021. **117**(7): p. 2173-2184.
36. Li, Y., et al., *Wear patterns and mechanisms of sialon ceramic end-milling tool during high speed machining of nickel-based superalloy.* Ceramics International, 2021. **47**(4): p. 5690-5698.
37. Holmberg, J., et al., *Selection of milling strategy based on surface integrity investigations of highly deformed Alloy 718 after ceramic and cemented carbide milling.* Journal of Manufacturing Processes, 2020. **58**: p. 193-207.
38. Hadi, M., et al., *Comparison between up-milling and down-milling operations on tool wear in milling Inconel 718.* Procedia Engineering, 2013. **68**: p. 647-653.
39. Pittalà, G. and M. Monno, *A new approach to the prediction of temperature of the workpiece of face milling operations of Ti-6Al-4V.* Applied Thermal Engineering, 2011. **31**(2-3): p. 173-180.
40. Matos, F.J.M., *Hard turning of Inconel 718 using PCBN tools*, in *DEMEC - FEUP*. 2022, UP.
41. Khader, I., A. Renz, and A. Kailer, *A wear model for silicon nitride in dry sliding contact against a nickel-base alloy.* Wear, 2017. **376**: p. 352-362.